AFRL-AFOSR-VA-TR-2023-0238

Detonation Wave Propagation in an Unwrapped RDE Channel

Yu, Kenneth
MARYLAND UNIV COLLEGE PARK
230 W 41ST STREET FL 7
NEW YORK, NY,
US

12/30/2022
Final Technical Report

Air Force Research Laboratory
Air Force Office of Scientific Research
Arlington, Virginia 22203
Air Force Materiel Command

REPORT DOCUMENTATION PAGE

PLEASE DO NOT RETURN YOUR FORM TO THE ABOVE ORGANIZATION.

1. REPORT DATE	2. REPORT TYPE	3. DATES COVERED	
20221230	Final	START DATE 20161201	END DATE 20211231

4. TITLE AND SUBTITLE
Detonation Wave Propagation in an Unwrapped RDE Channel

5a. CONTRACT NUMBER	5b. GRANT NUMBER	5c. PROGRAM ELEMENT NUMBER
	FA9550-17-1-0086	61102F
5d. PROJECT NUMBER	**5e. TASK NUMBER**	**5f. WORK UNIT NUMBER**

6. AUTHOR(S)
Kenneth Yu

7. PERFORMING ORGANIZATION NAME(S) AND ADDRESS(ES)
MARYLAND UNIV COLLEGE PARK
230 W 41ST STREET FL 7
NEW YORK, NY
US

8. PERFORMING ORGANIZATION REPORT NUMBER

9. SPONSORING/MONITORING AGENCY NAME(S) AND ADDRESS(ES)	10. SPONSOR/MONITOR'S ACRONYM(S)	11. SPONSOR/MONITOR'S REPORT NUMBER(S)
Air Force Office of Scientific Research 875 N. Randolph St. Room 3112 Arlington, VA 22203	AFRL/AFOSR RTA1	AFRL-AFOSR-VA-TR-2023-0238

12. DISTRIBUTION/AVAILABILITY STATEMENT
A Distribution Unlimited: PB Public Release

13. SUPPLEMENTARY NOTES

14. ABSTRACT
The nature of the coupling between shock wave and combustion zone in a partially-open channel geometry is investigated experimentally and analytically. The channel geometry used in this investigation constitutes a canonical configuration, which simulates an unwrapped shape of a rotating detonation engine (RDE) combustor. In this canonical configuration, controlled reactants
are injected transversely from the channel base using a set of model injectors, and detonation waves are established from one or both ends of the channel at a controlled timing to simulate
RDE operation. The principal objective of the research is to build the scientific knowledge and the quantitative database for better understanding the physical processes that occur in RDE
combustors. For such a configuration, it is observed that there are substantial differences as well as similarities in measured detonation wave characteristics when compared to the previously
known properties of detonation waves, which are associated with a fully-confined duct geometry. While the similarities include mostly qualitative observations such as extremely complex threedimensional detonation structure, unstable and oscillating lead shock wave strength, existence of the triple points and detonation cells, etc., there are also some notable differences in the wave
structure, the characteristic cell size, and the characteristic wave speed associated with various reactant mixtures using the present configuration. These differences are attributed not only to the
partial confinement effect but also to the effects of non-uniform mixing and the injector dynamic response associated with the particular boundary conditions. While the state of mixing and the
injector dynamics control the relative location of the detonation wave heat release, the detonation wave properties are sensitively affected by the degree of shock wave-heat release coupling,
which is further amplified by the partial confinement effect in the present configuration. The overall research effort comprised of the following technical elements: (1) comparison of performances from optimized ideal thermodynamic cycles, (2) linear model detonation engine (LMDE) experiments characterizing detonation transit phase and injection refresh phase in model RDE combustors, (3) development of partial mixture detonation model for quantifying the effect of incomplete mixing in experimentally observed detonation wave speed, and (4) effects of propellants and products composition on detonation wave characteristics. The research results for each of these program elements are summarized in this report.

15. SUBJECT TERMS

16. SECURITY CLASSIFICATION OF:			17. LIMITATION OF ABSTRACT	18. NUMBER OF PAGES
a. REPORT U	b. ABSTRACT U	c. THIS PAGE U	UU	47

19a. NAME OF RESPONSIBLE PERSON	19b. PHONE NUMBER *(Include area code)*
CHIPING LI	426-8574

Final Report

on

Detonation Wave Propagation in an Unwrapped RDE Channel

Grant Number: FA9550-17-1-0086

Prepared for
AIR FORCE OFFICE OF SCIENTIFIC RESEARCH

Program Manager:
Dr. Chiping Li

For the Period
01 December 2016 to 31 December 2020

Submitted by:

Principal Investigator:
Ken H. Yu
Department of Aerospace Engineering
University of Maryland
College Park, MD 20742
yu@umd.edu
(301) 405-1333

TABLE OF CONTENTS

Detonation Wave Propagation in an Unwrapped RDE Channel

J. Burr, R. Fievisohn, S. Redhal, M. Chang, and K.H. Yu
Department of Aerospace Engineering
University of Maryland
College Park, MD 20742

1.0 SUMMARY

The nature of the coupling between shock wave and combustion zone in a partially-open channel geometry is investigated experimentally and analytically. The channel geometry used in this investigation constitutes a canonical configuration, which simulates an unwrapped shape of a rotating detonation engine (RDE) combustor. In this canonical configuration, controlled reactants are injected transversely from the channel base using a set of model injectors, and detonation waves are established from one or both ends of the channel at a controlled timing to simulate RDE operation. The principal objective of the research is to build the scientific knowledge and the quantitative database for better understanding the physical processes that occur in RDE combustors. For such a configuration, it is observed that there are substantial differences as well as similarities in measured detonation wave characteristics when compared to the previously known properties of detonation waves, which are associated with a fully-confined duct geometry. While the similarities include mostly qualitative observations such as extremely complex three-dimensional detonation structure, unstable and oscillating lead shock wave strength, existence of the triple points and detonation cells, etc., there are also some notable differences in the wave structure, the characteristic cell size, and the characteristic wave speed associated with various reactant mixtures using the present configuration. These differences are attributed not only to the partial confinement effect but also to the effects of non-uniform mixing and the injector dynamic response associated with the particular boundary conditions. While the state of mixing and the injector dynamics control the relative location of the detonation wave heat release, the detonation wave properties are sensitively affected by the degree of shock wave-heat release coupling, which is further amplified by the partial confinement effect in the present configuration. The overall research effort comprised of the following technical elements: (1) comparison of performances from optimized ideal thermodynamic cycles, (2) linear model detonation engine (LMDE) experiments characterizing detonation transit phase and injection refresh phase in model RDE combustors, (3) development of partial mixture detonation model for quantifying the effect of incomplete mixing in experimentally observed detonation wave speed, and (4) effects of propellants and products composition on detonation wave characteristics. The research results for each of these program elements are summarized in this report.

2.0 INTRODUCTION

Rotating detonation engine (RDE) is one of the most promising combustor concepts that can revolutionize the future propulsion and power systems. [1-6] RDE has a detonation-based thermodynamic cycle, which can provide substantial design benefits as well as thermodynamic efficiency improvements over the Brayton-cycle engines. There are a number of on-going investigations studying various aspects of RDE, from understanding basic physics to integrating RDE to aerospace platforms.

2.1. Background and Anatomy of Rotating Detonation Engine

A typical RDE combustor (Fig. 2.1) is shaped like an annular duct bounded by the upstream end connected to an "acoustically-closed" inlet annulus fitted with a set of injectors for bringing in the fresh reactants and the downstream end connected to an "acoustically-open" nozzle annulus, through which the product gases can be discharged. For clarification, we use the term "acoustically-closed" to describe the boundary where the minimum cross-sectional area is less than 50% of the combustor cross-sectional area and the term "acoustically-open" to describe the boundary where the throat area is greater than or equal to 50% of the combustor cross-sectional area. Thus, a shock wave would likely reflect as a shock wave from the inlet boundary (referred to as the "base") and would reflect as expansion waves from the combustor exit (referred as the "top" in the current experimental setup).

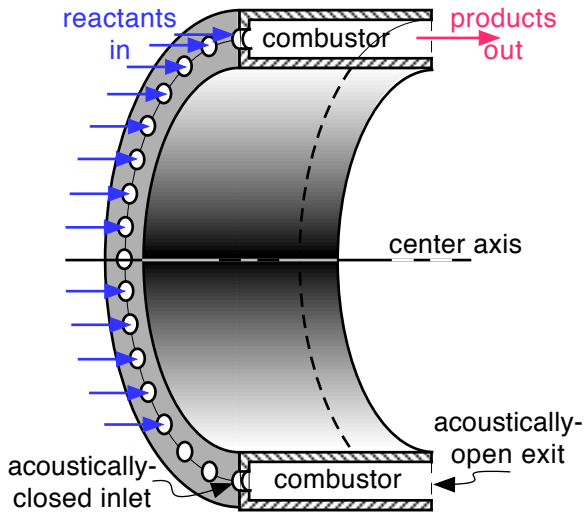

Figure 2.1. Sectional view of a typical RDE combustor (annular)

In RDE combustors, a self-sustaining shock wave propagates around the annulus in the azimuthal or the tangential direction compressing the freshly injected reactants that have been mixing around the base region. The compressive heating caused by the shock wave as well as the shock enhanced mixing initiates rapid chemical reaction processes, that lead to an interaction between the combustion zone and the shock wave. This group of "shock-flame" structure can be called a detonation wave as it propagates at a supersonic speed relative to the freshly injected reactants. The nature of the shock-flame interaction process affects the detonation wave characteristics such as the characteristic pressure rise and the wave speed. If a sufficient amount

of heat release were established close to the shock wave front, then the resulting volumetric expansion could power the wave speed theoretically up to the Chapman-Jouguet condition.

As a detonation wave propagates circumferentially along the base of an annular chamber, it also sets up a high-pressure pulse that can temporarily obstruct the injection process at the base. Subsequent injection of the reactants and the ensuing detonation wave repeat the cyclic process at a high repetition rate. The flow behavior in each RDE cycle comprises of two distinctive phases corresponding to different physical processes. In one part of the cycle, a detonation wave propagates over the freshly injected reactants, while in the other part, injection refreshes following the detonation wave passage.

2.2. Scope and Research Objectives

This study was motivated by the desire to better understand the key physical processes that occur in RDE combustors and provide more detailed experimental data on the relevant detonation wave characteristics. The goal is to build the qualitative scientific knowledge, quantitative database, and fundamental understanding that can help RDE combustor design, testing data analysis, and performance prediction as well as the flow structure and detonation wave modeling directly relevant to an RDE configuration. To achieve this goal, detonation research is conducted using a canonical configuration that captures the essence of the RDE flowfield. A linear channel simulating an unwrapped RDE combustor is considered with extensive diagnostics and measurements.

Figure 2.2 illustrates a schematic of an unwrapped RDE combustor and a schlieren image obtained using such configuration.

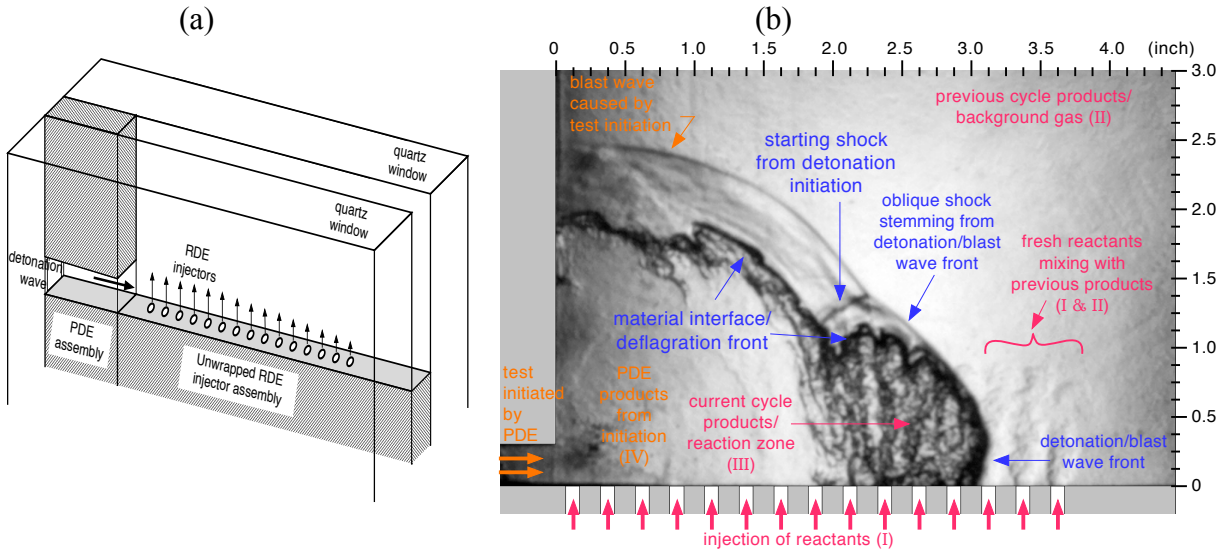

Figure 2.2. Unwrapped RDE combustor configuration
(a) illustration of the setup, and (b) schlieren image of the flowfield

3.0 RDE MODELING AND THEORETICALCONSIDERATIONS

3.1. Ideal Thermodynamic Cycles

Cycle analysis is a study of thermodynamic behavior of the working fluid as it flows through an engine. Its purpose is to estimate the performance parameters, such as thrust and specific fuel consumption in terms of design requirements, which include:

- design limitation, such as maximum combustor temperature (T_4) etc.
- operating conditions, such as ambient pressure (p_∞), temperature (T_∞), etc.
- design choices, such as compression pressure ratio (π_c), etc.

Cycle analysis can provide a "rubber engine" performance. In other words, the computed characteristics only represent the potential performance, not actual. The real engine performance would be determined by its geometry and operating parameters. Some examples of standard thermodynamic cycles related to chemical propulsion in air and space are summarized and illustrated in the following (ideal cycles):

- Brayton Cycle
  - an approximate representation of idealized jet engine cycles, such as gas turbines, ramjets, scramjets, etc. (characterized by constant-pressure heat addition process)

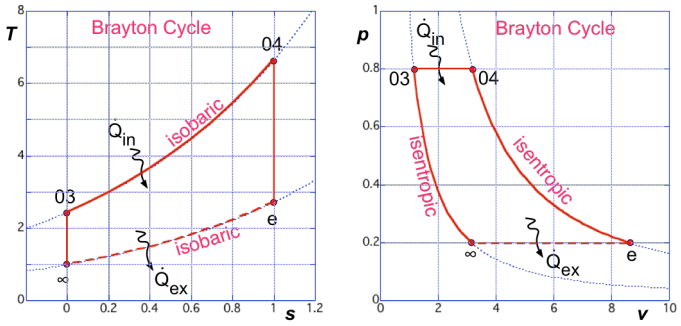

Figure 3.1. Brayton cycle T-s and p-v diagrams

The thermodynamic states are presented in Fig. 3.1 and include the following processes:

∞ → 03: intake & compression
03 → 04: heat release (assumed at constant pressure)
04 → e: turbine/nozzle expansion
e → ∞: exhaust (constant pressure)

- Humphrey Cycle
  - an approximate representation of idealized detonation engine cycles, even though detonative combustion is not a constant-volume process (this is in similar spirit as assuming Brayton cycle for jet engines, even though deflagration is not a constant-pressure process either)

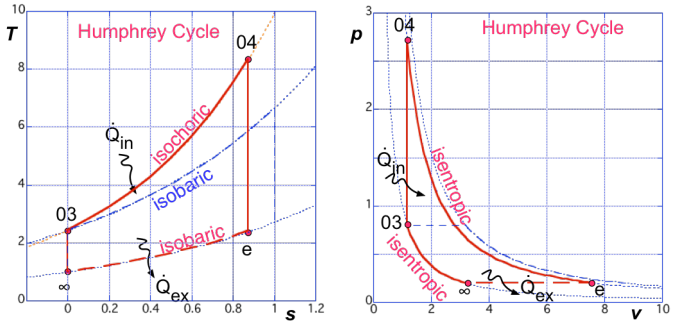

Figure 3.2. Humphrey cycle T-s and p-v diagrams

The thermodynamic states are presented in Fig. 3.2, and include the following processes:

∞ → 03: intake & compression
03 → 04: heat release (assumed at constant volume)
04 → e: turbine/nozzle expansion
e → ∞: exhaust (constant pressure)

- Rocket
  - cycle analysis is somewhat uncommon since the thermodynamic state of "working fluid" (the propellants) in steady operation is already known. In case of non-traditional engines, the cycle analysis could be useful. In any rate, the actual propulsion performance will be subjected to many physical constraints, such as pressure and temperature limitations.

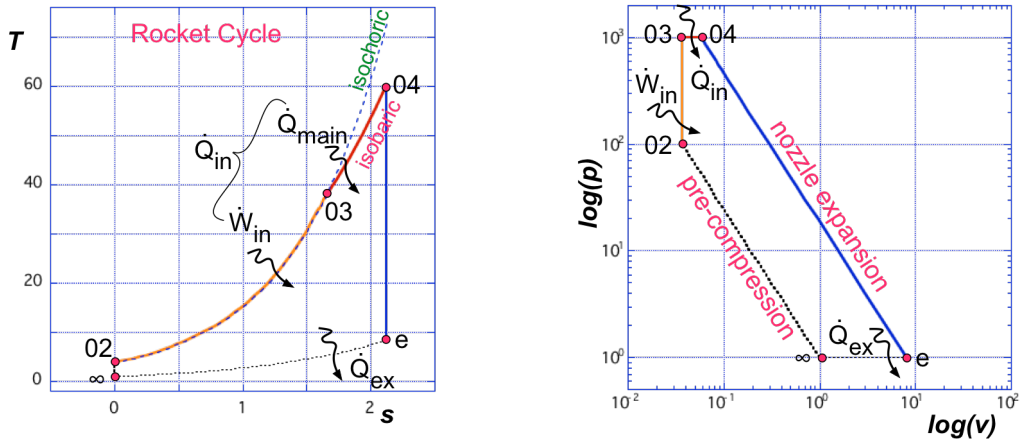

Figure 3.3. T-s and p-v diagrams for a typical rocket-based cycle

The thermodynamic states are presented in Fig. 3.3, and include the following processes:

∞ → 02:	stored propellants in tanks (may be considered as pre-compression)
02 → 03	propellants compression, using turbo-pumps
03 → 04	heat release process in thrust chamber (typically, isobaric)
04 → e:	nozzle expansion (assumed isentropic for ideal cycle analysis)

Note: Here, the Station (∞) represents a hypothetical state with the same pressure as in the Station (e) and the same entropy as in the Station (02).

Modeling Detonation in Ideal Cycle Analysis

For estimating relevant thermodynamic cycle performance, one approach is to approximate the detonation engine thermodynamic cycle behavior using standard Humphrey Cycle with isochoric heat addition model or more specialized piston-cylinder model such as Fickett-Jacobs Cycle. [7] Another simple but practical approach is to assume that one can combine a variable amount of isentropic pre-compression followed by Chapman-Jouguet (CJ) detonation wave which provides additional compression and heat release. This allows theoretical optimization of compression amount that may maximize the work output for the given cycle.

For physical description of flow structure and behavior associated with the propagating detonation wave, one-dimensional ZND (Zel'dovich-von Neumann-Döring) model can be utilized for qualitative insight, while for calculating the thermodynamic properties at various states any established chemical equilibrium code may yield a reasonable estimate of more quantitative accuracy.

For the ZND model, illustrated in Fig. 3.4, a detonation wave is treated as a shock wave (normal) followed by an exothermic reaction zone, which in turn provides energy needed to sustain the shock wave speed. In a wave-referenced frame, the supersonic reactant flow (State 2) is shocked down to a subsonic speed (State 3) and then the exothermic reaction of the elevated-temperature reactants causes thermal choking (State 4) via Rayleigh heating. This yields the same detonation speed as in the CJ theory. To facilitate the 1-D analysis and computation, one can start from the known values of CJ detonation properties, such as detonation Mach number, M_{CJ}.

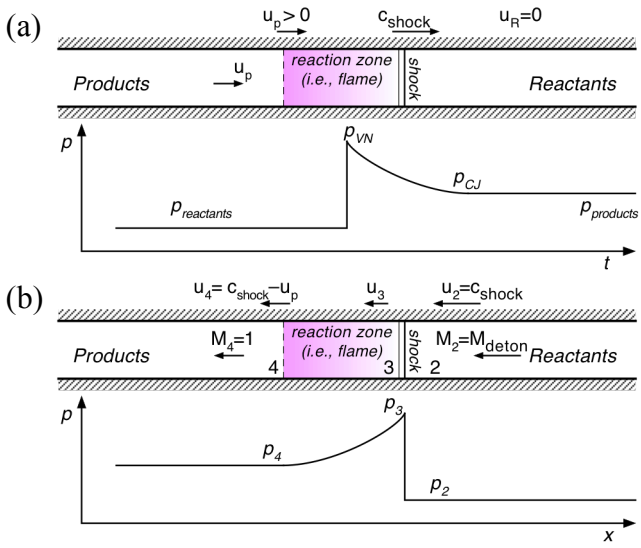

Figure 3.4. Illustration of ZND model.
(a) observer-reference, pressure-time sequence,
(b) wave-reference, pressure distribution in space

Here, the following numbering system is used to identify thermodynamic state associated with the propulsion cycle:
State (2) – thermodynamic states of the reactants, but in the wave-referenced frame ($M_2 = M_{CJ}$)
State (3) – thermodynamic state of the shocked reactants in the wave-referenced frame
State (4) – thermodynamic state of the products immediately after the detonation wave passage

- Thermodynamic state across a shock: from State (2) to State (3)

One can use the normal shock equations to go from State (2) to State (3). For example, the State (2) corresponds to the reactant state, which is flowing at the CJ detonation speed in the wave-referenced frame. To obtain the intermediate points between the States (2) and (3), one can use the set of equations for Rankine-Hugoniot, or Hugoniot with no heat release.

Normal shock relations

$$M_3 = \sqrt{\frac{M_2^2 + \frac{2}{\gamma - 1}}{\frac{2\gamma}{\gamma - 1} M_2^2 - 1}} \qquad p_3 = p_2 \left[1 + \left(\frac{2\gamma}{\gamma + 1} \right) \left(M_2^2 - 1 \right) \right] \qquad T_3 = T_2 \left[\frac{\left(1 + \frac{\gamma - 1}{2} M_2^2 \right) \left(\frac{2\gamma}{\gamma - 1} M_2^2 - 1 \right)}{\frac{(\gamma + 1)^2}{2(\gamma - 1)} M_2^2} \right]$$

$$\upsilon_3 = \upsilon_2 \left(\frac{T_3 / T_2}{p_3 / p_2} \right) \qquad \frac{s_3 - s_2}{R} = \frac{\gamma}{\gamma - 1} \ln \left[\frac{2}{(\gamma + 1) M_2^2} + \left(\frac{\gamma - 1}{\gamma + 1} \right) \right] + \frac{1}{\gamma - 1} \ln \left[\frac{2\gamma M_2^2}{\gamma + 1} - \left(\frac{\gamma - 1}{\gamma + 1} \right) \right]$$

$$p_{03} = p_{02} \frac{\left[\left(\frac{\gamma+1}{2} M_2^2\right) \Big/ \left(1 + \frac{\gamma-1}{2} M_2^2\right)\right]^{\frac{\gamma}{\gamma-1}}}{\left[\frac{2\gamma}{\gamma+1} M_2^2 - \left(\frac{\gamma-1}{\gamma+1}\right)\right]^{\frac{1}{\gamma-1}}} \qquad T_{03} = T_{02} = T_2 \left(1 + \frac{\gamma-1}{2} M_2^2\right)$$

- Thermodynamic state across a combustion wave: from State (3) to State (4)

To generate a continuous path from State (2) to State (3), one can use the equations for Rankine-Hugoniot. However, it can be noted that only the continuity equation is satisfied continuously along this path. The momentum and energy equations are satisfied only at the two end points – State (2) and State (3). They're not in equilibrium while transitioning along the path.

Rankine-Hugoniot Relations

$$\frac{p}{p_2} = \frac{\left(\frac{\gamma+1}{\gamma-1}\right) - \frac{\upsilon}{\upsilon_2}}{\left(\frac{\gamma+1}{\gamma-1}\right)\frac{\upsilon}{\upsilon_2} - 1} \qquad \frac{\upsilon}{\upsilon_2} = \frac{\frac{p}{p_2} + \left(\frac{\gamma+1}{\gamma-1}\right)}{\left(\frac{\gamma+1}{\gamma-1}\right)\frac{p}{p_2} + 1} \qquad \frac{T}{T_2} = \frac{\frac{p}{p_2}\left[1 + \left(\frac{\gamma-1}{\gamma+1}\right)\frac{p}{p_2}\right]}{\frac{p}{p_2} + \left(\frac{\gamma-1}{\gamma+1}\right)}$$

$$\frac{s - s_2}{R} = \ln\left[\frac{\left(T \Big/ T_2\right)^{\frac{\gamma}{\gamma-1}}}{\left(p \Big/ p_2\right)}\right] \qquad h = h_2 + \frac{1}{2}(p - p_2)(\upsilon + \upsilon_2)$$

- Obtaining thermodynamic path from State (3) to State (4)

One can use Rayleigh flow equations to generate a continuous path from State (3), which corresponds to subsonic flow in wave-reference frame, to State (4), which is the thermally choked point. The simplest way to do this is to incrementally advance the flow Mach number from M_3 to M_4, which is equal to unity. Then, one can find the thermodynamic properties of the intermediate states as a function of the intermediate Mach number, while using State (4) as the reference point.

First, one needs to obtain the thermally choked State (4) in order to use it as a reference state. This can be done using the known properties at either State (2) or State (3):

$$T_{04} = T_0^* = T_{03}\frac{\left(1+\gamma M_3^2\right)^2}{\left(\gamma+1\right)M_3^2\left[2+(\gamma-1)M_3^2\right]}$$

$$p_4 = p^* = p_3\frac{1+\gamma M_3^2}{\gamma+1}$$

$$T_4 = T^* = T_3\frac{(1+\gamma M_3^2)^2}{(\gamma+1)^2 M_3^2}$$

$$\upsilon_4 = \upsilon^* = \upsilon_3\frac{1+\gamma M_3^2}{(\gamma+1)M_3^2}$$

$$p_{04} = p_{04}^* = p_{03}\frac{(1+\gamma M_3^2)}{(\gamma+1)}\left[\frac{\gamma+1}{2+(\gamma-1)M_3^2}\right]^{\frac{\gamma}{\gamma-1}}$$

Now, using the properties at State (4) as a reference, all the intermediate states can be specified as a function of Mach number, marching from M_3 to M_4, incrementally.

Rayleigh Flow Equations

$$\frac{p}{p_4} = \frac{\gamma+1}{1+\gamma M^2} \qquad \frac{T}{T_4} = \frac{(\gamma+1)^2 M^2}{(1+\gamma M^2)^2}$$

$$\frac{\upsilon}{\upsilon_4} = \frac{(\gamma+1)M^2}{1+\gamma M^2}$$

$$\frac{s-s_3}{R} = \ln\left[\left(\frac{M}{M_3}\right)^{\frac{2\gamma}{\gamma-1}}\left(\frac{1+\gamma M_3^2}{1+\gamma M^2}\right)^{\frac{\gamma+1}{\gamma-1}}\right]$$

$$\frac{p_0}{p_{04}} = \frac{(\gamma+1)}{(1+\gamma M^2)}\left[\frac{2+(\gamma-1)M^2}{\gamma+1}\right]^{\frac{\gamma}{\gamma-1}} \qquad \frac{T_0}{T_{04}} = \frac{(\gamma+1)M^2\left[2+(\gamma-1)M^2\right]}{(1+\gamma M^2)^2}$$

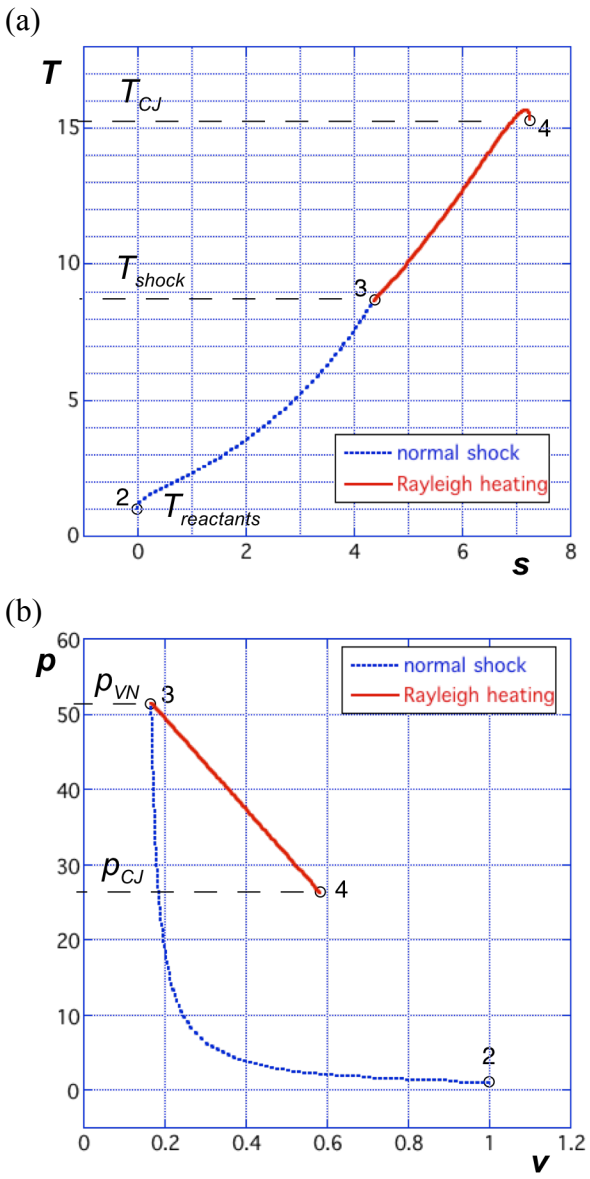

Figure 3.5. Illustration of T-s and p-v diagrams using ZND detonation model (γ=1.35)

Typical traces of T-s and p-v diagrams are shown in Fig. 3.5, using ZND detonation model analysis without any pre- isentropic compression. For example, the process from State (2) to State (3) in this figure represents the shock compression within the ZND detonation wave structure.

Comparison of Optimized Thermodynamic Cycles

For ideal cycles involving constant specific heat ratio (i.e., γ=constant), it is straightforward to show that the specific work (or specific thrust) can be maximized under given conditions and the corresponding thermodynamic efficiency can be obtained for that particular condition. For instance, if we assume that the maximum flow temperature is limited due to the material consideration and the minimum flow temperature occurs at the inlet state (∞), a temperature-constrained work optimization problem can be established. Table 3.1 summarizes the results for ideal Brayton cycle and ideal Humphrey cycle, that each produces maximum specific work, respectively.

Table 3.1. Comparison of Ideal Thermodynamic Cycles operating between two temperature limits

	Brayton cycle	Humphrey cycle
Combustor inlet temperature, T_3	$T_3 = T_{\max}^{1/2} T_{\min}^{1/2}$	$T_3 = T_{\max}^{1/(\gamma+1)} T_{\min}^{\gamma/(\gamma+1)}$
Optimum compression ratio Π_{comp}	$\left(\frac{p_3}{p_\infty}\right) = \left(\frac{T_{\max}}{T_{\min}}\right)^{\frac{\gamma}{2(\gamma-1)}}$	$\left(\frac{p_3}{p_\infty}\right) = \left(\frac{T_{\max}}{T_{\min}}\right)^{\frac{\gamma}{(\gamma+1)(\gamma-1)}}$
Nozzle exit temperature, T_e	$T_e = T_3 = T_{\max}^{1/2} T_{\min}^{1/2}$	$T_e = T_3 = T_{\max}^{1/(\gamma+1)} T_{\min}^{\gamma/(\gamma+1)}$
Thermo-dynamic efficiency, η_{th}	$\eta_{th} = 1 - \left(\frac{T_{\min}}{T_{\max}}\right)^{1/2}$	$\eta_{th} = 1 - \gamma \frac{\left[1 - \left(\frac{T_{\max}}{T_{\min}}\right)^{\frac{-1}{\gamma+1}}\right]}{\left[\left(\frac{T_{\max}}{T_{\min}}\right)^{\frac{\gamma}{\gamma+1}} - 1\right]}$
Specific work, w_{sp}	$w_{\max} = \frac{\gamma R}{\gamma-1}\left(\sqrt{T_{\max}} - \sqrt{T_{\min}}\right)^2$	$w_{\max} = \left(\frac{R}{\gamma-1}\right)\left[T_{\max} + \gamma T_{\min} - (\gamma+1)\, T_{\max}^{1/(\gamma+1)} T_{\min}^{\gamma/(\gamma+1)}\right.$

The respective thermodynamic efficiencies are compared in Fig. 3.6 for a constant γ case. The results shows there is relatively little gain associated with using the Humphrey cycle over the Brayton cycle. It should also be noted that there is some specific-work penalty of using the Humphrey cycle. These results suggest that adapting a constant-volume heat addition process for the sole purpose of thermodynamic efficiency improvement may not be that practical after all.

On the other hand, if one compares the required compression ratio for maximum specific work, there may be substantial benefits of using the Humphrey cycle over the Brayton cycle. Figure 3.7 focuses on this aspect of the cycle comparison. The amount of "gain" associated with the reduced compression requirement of a Humphrey cycle increases with the temperature ratio.

From the system engineering perspective, this advantage could be important especially as one moves toward the mission where the performance limitation stems from the compression requirement. It can also be noted that possible benefits of additional compression associated with detonation wave may be useful if the required compression ratio is very high for the optimum work.

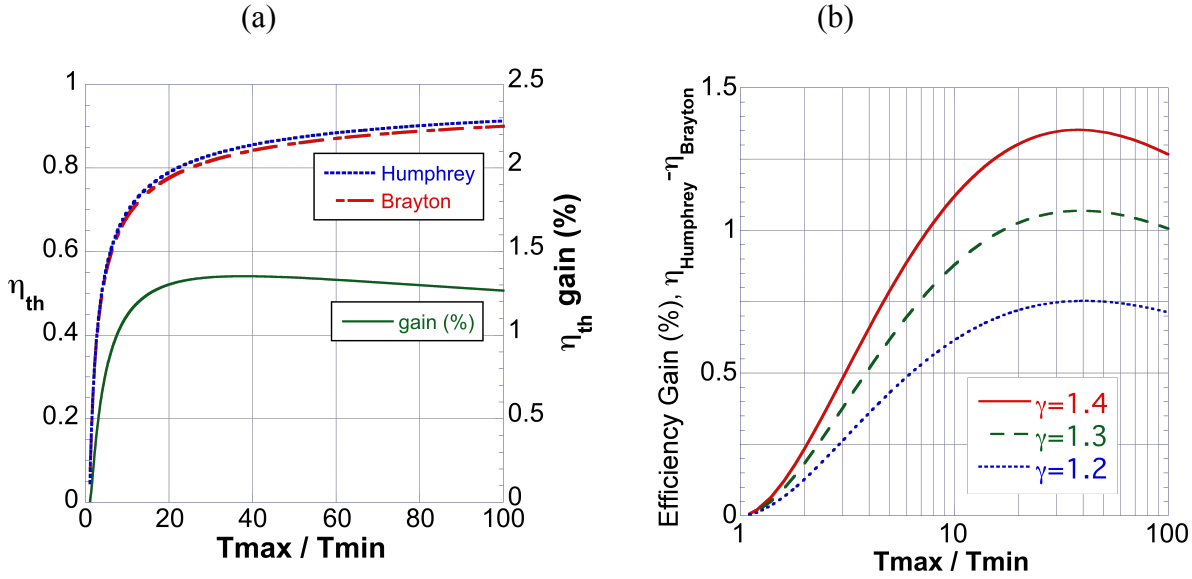

Figure 3.6. Thermodynamic efficiency gain of Humphrey cycle over Brayton cycle. (a) efficiency .vs. temperature ratio, and (b) efficiency gain as a function of γ

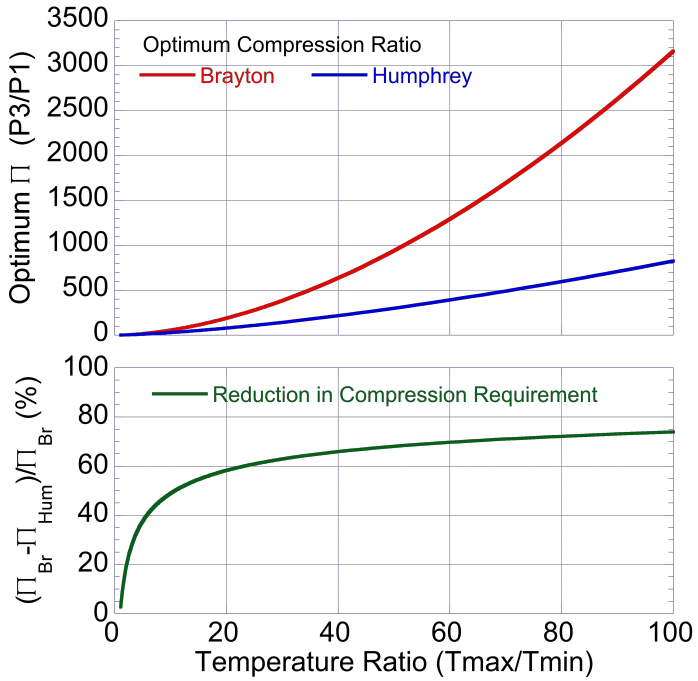

Figure 3.7. Compression ratio needed for optimum work production for Brayton and Humprey cycles, respectively.

3.2 MOC Analysis of Detonation Wave in RDE

(from Robert Fievisohn's Ph.D. thesis, 2016)

This work is focused on developing and applying theoretical models to aid in the design and understanding of Rotating Detonation Engines (RDEs). In an RDE, a detonation wave travels circumferentially along the bottom of an annular chamber, where continuous injection of fresh reactants sustains the detonation wave. RDEs are currently being designed, tested, and studied as a viable option for developing a new generation of turbine and rocket engines that make use of detonation heat release. One of the main challenges in the development of RDEs is to understand the complex flowfield inside the annular chamber. While simplified models are desirable for obtaining timely performance estimates for design analysis, one-dimensional models may not be adequate as they do not provide flow structure information. In this work, a two-dimensional physics-based model is developed, which is capable of modeling the curved oblique shock wave, exit swirl, counter-flow, detonation inclination, and varying pressure along the inflow boundary. This is accomplished by using a combination of shock-expansion theory, Chapman-Jouguet detonation theory, the Method of Characteristics (MOC), and other compressible flow equations to create a shock-fitted numerical algorithm and generate an RDE flowfield. Typical examples of the computed flowfield are shown in Figs. 3.8 and 3.9. This novel approach provides a numerically efficient model that can provide performance estimates as well as details of the large-scale flow structures in seconds on a personal computer. Results from this model are validated against high-fidelity numerical simulations that may require a high-performance computing framework to provide similar performance estimates. This work provides a designer a new tool to conduct large-scale parametric studies to optimize a design space before conducting computationally-intensive, high-fidelity simulations that may be used to examine additional effects. This work not only bridges the gap between simple one-dimensional models and high-fidelity full numerical simulations, but it also provides an effective tool for understanding and exploring RDE flow processes.

More details of this work can be found in the Ph.D. thesis by Robert Fievisohn [8]

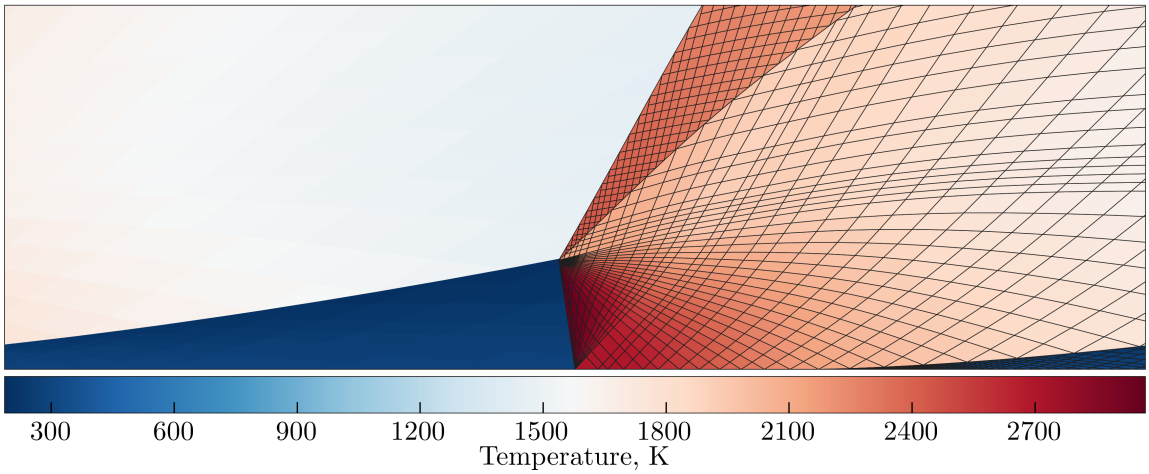

Figure 3.8. Temperature contour for unwrapped RDE one-wave solution. P_0=10atm, T_0=300K, C=47.88cm, W=1.27cm. H=15.24cm, A_t/A_w=0.3, ϕ=1

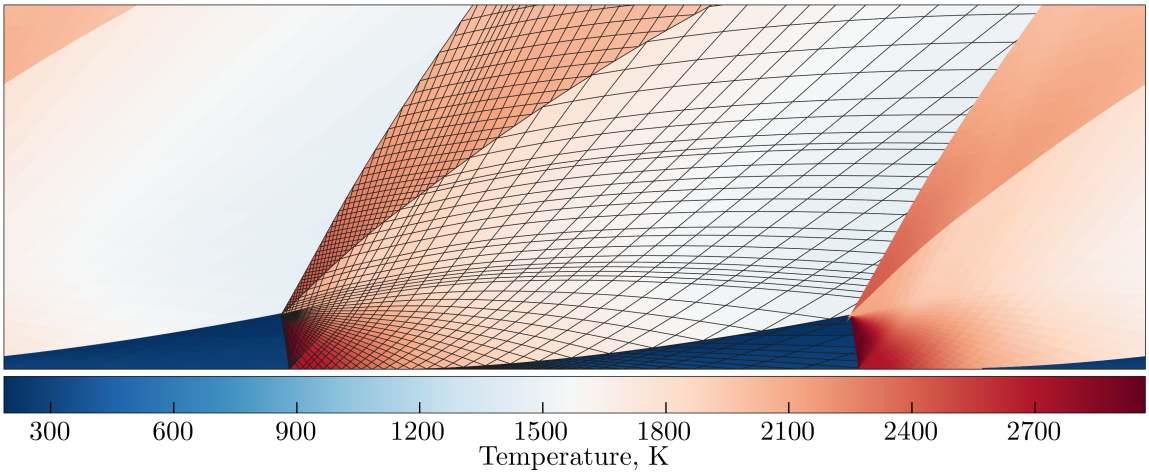

Figure 3.9. Temperature contour for unwrapped RDE two-wave solution. P_0=10atm, T_0=300K, C=47.88cm, W=1.27cm. H=15.24cm, A_t/A_w=0.3, ϕ=1

Objectives

This study is for complementing the experimental study summarized in the next section. The goal is to establish a new analytical framework for estimating RDE performance parametrically and for guiding the experimental investigation. The specific objectives are to analyze the flow structure in simplified RDE flowfield, and identify important physical parameters and technical issues relevant to RDE operation.

Modeling Approach

The approach here is to model the internal flowfield of an RDE using a simple canonical configuration of detonation wave being bounded by non-reacting products from the previous cycle on the upper boundary and porous wall on the lower boundary that is acoustically closed but allows reactants inflow. This configuration would be analogous to the steady-state behavior of detonation wave propagating in crossflow of reactants at a given height.

A novel, two-dimensional, physics-based modeling approach is developed using a combination of shock-expansion theory, Chapman-Jouguet detonation theory, the Method of Characteristics (MOC), and other concepts from compressible flow theory for numerically generating an RDE flowfield. This model required the development of the first mass injection boundary condition for the two-dimensional Method of Characteristics as well as an extension of the slip line boundary condition to rotational flowfields. An improved numerical algorithm for solving the characteristic and compatibility relations along a streamline has been developed to greatly increase the accuracy over more traditional MOC algorithms in flows with large entropy gradients. A unique marching algorithm capable of marching out multiple regions concurrently along with MOC based interpolation routines have also been developed to model the unique conditions inside an RDE. Results from this model are validated against high-fidelity numerical simulations and are shown to provide similar performance estimates. The solver is used to perform a preliminary analysis of an ethylene-air RDE and several significant design parameters are identified in order to correctly size the engine and maximize performance.

3.3 Partial Mixture Detonation Model
(from Jason Burr's Ph.D. thesis, 2020)

In typical RDE experiments, the observed detonation wave speed tends to be much lower than the characteristic Chapman-Jouguet (CJ) detonation wave speed associated with the reactant mixture. To provide physical insights into such observation, the expected detonation wave speed was estimated assuming the reactants are incompletely mixed. This model assumes that only a certain fraction of the potential heat release is coupled to the detonation wave.

In one-dimensional approximation, a detonation wave can be modeled as a normal shock wave followed by a zone of exothermic reaction that sustains the shock wave speed (ZND). A typical steady-state analysis in a wave-referenced frame assumes that the incoming reactants approaching the wave initially at a supersonic speed get shocked down to a subsonic speed. Subsequently, the elevated-temperature flow reacts exothermically and causes thermal choking via Rayleigh heating. The induction time is not important in the one-dimensional analysis, as the thermal choking depends only on the total amount of heat release. The solution forces the products to reach the sonic speed in the wave-referenced frame, and this yields the same detonation speed as the CJ theory. (CJ) It is well known that the CJ detonation wave can be analytically obtained using Rankine-Hugoniot solution for various amounts of heat release for various compositions of reactants and products.

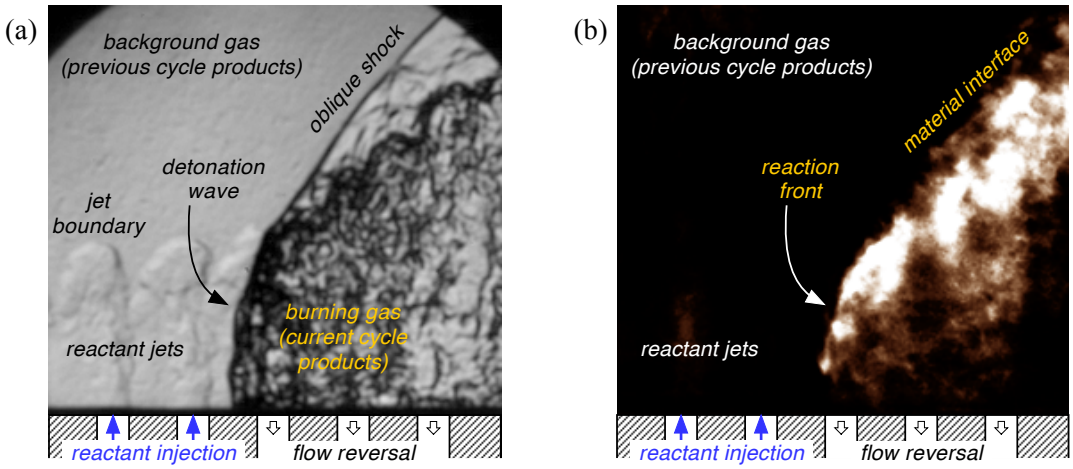

Figure 3.10. Flow structure depicted in a wave stationary frame of reference (i.e., flow from left to right) (a) schlieren image showing density gradients, and (b) luminescence image showing the reaction zone

In an RDE configuration, however, the affected volume of the products is only partially confined by the channel geometry, allowing the flow expansion toward the downstream direction as well as the potential flow reversal into the injector plane. As a result, only the amount of heat release that is closely coupled to the lead shock wave front may play a role in driving the actual detonation wave speed. Figure 3.10 shows both a schlieren image and a luminescence image, associated with a typical detonation wave propagating in our linear channel set-up. It can be clearly observed that the zone of luminescence is stretched broadly into the product region following the detonation and the associated oblique shock wave. This indicates that some of the heat release may indeed be distributed over the expanding flow region, and not all heat release may be directly coupled to the lead shock wave front. Then, only the specific portion of the total

heat release, which is close-coupled to the lead shock wave front and is locally choking the shocked flow, is expected to contribute in establishing the detonation wave speed.

Considering only that amount of heat release closely-coupled to the shock wave before the flow expansion will affect the driving of the wave speed, we need to separate the contribution of total heat release into the detonation reaction part which is closely coupled and the deflagration part post the initial expansion of the flow. A simple model to assess the variation in CJ detonation wave speed due to partial detonation reaction is illustrated in Fig. 3.11, and the corresponding pseudo-code for Cantera implementation is shown in Fig. 3.12.

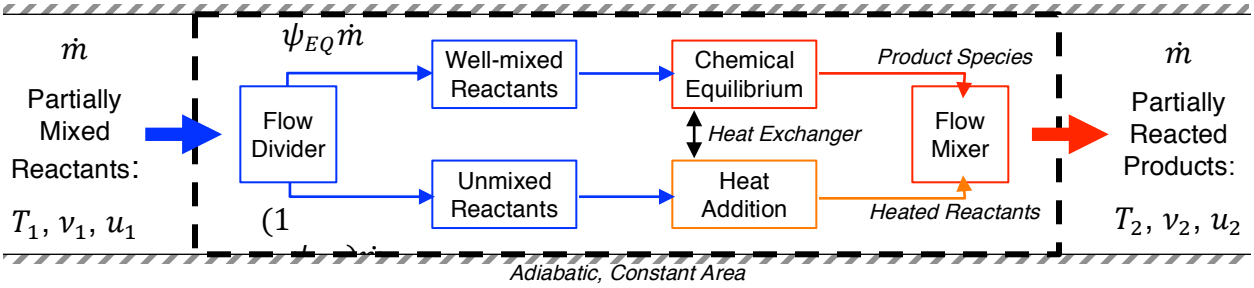

Figure 3.11. Partial mixture detonation model

The extent of mixing is quantified with the partial fraction parameter ψ_{EQ}, which represents the mass fraction that detonates before the flow expansion thus contributing to the driving of the detonation wave front. This rapidly reacted mass fraction is assumed to be in thermodynamic equilibrium with the yet unreacted flow at the unique final state given by T_2 and ν_2, yielding a species composition $\bar{Y}_{EQ}$. The remaining fraction of unmixed reactants can be brought to the same temperature and specific volume for wave speed calculation; although the remaining fraction may be allowed to react after the flow started expanding resulting in deflagration front that does not contribute to initial thermal choking.

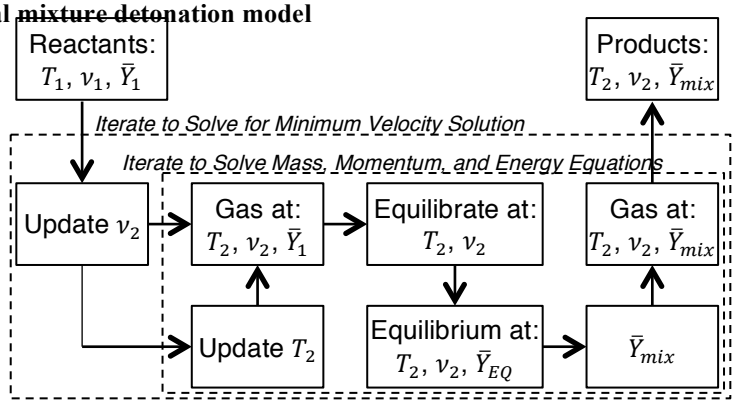

Figure 3.12. Pseudo-code for Cantera-based iterative partial mixture detonation model.

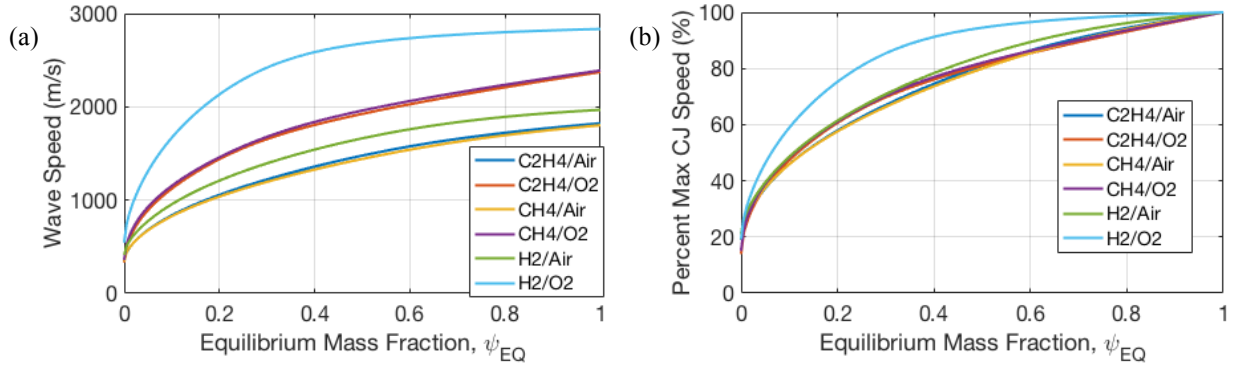

Figure 3.13. CJ detonation wave speed in RDE setup associated with partial fraction detonation model

Mixing-limited detonation wave speeds were calculated for a number of stoichiometric reactant mixtures and are shown in Fig. 3.13. Figure 3.13(a) shows the value of these CJ speeds, while Fig. 3.13(b) normalizes the CJ speed with the expected CJ speed for a well-mixed and fully reacted mixture. For all reactant mixtures the CJ speed approached the bulk sound speed of the reactants as the equilibrium mass fraction approached zero, and approached the well-mixed CJ speed for the mixture as the equilibrium mass fraction approached unity. In all cases the trend between CJ speed and equilibrium mass fraction, and by extension the amount of heat release to the flow, agrees well with the classic Rankine-Hugoniot calculation. Also, the behavior of C_2H_6 and C_3H_8 closely matched that of CH_4 and C_2H_4, although only two hydrocarbon fuels are displayed in Fig. 3.13 for clarity.

4.0 Characterization of Detonation Wave in Open Channel

(from Jason Burr's Ph.D. thesis, 2020)

Summary

In this work the propagation of various detonation waves through a flowfield analogous to RDE are studied experimentally. A canonical configuration that "unwraps" the RDE into a linear channel is used to examine the effects of reactant species, mixedness, heat release, and layer height on the structure and propagation characteristics of detonation in RDE. This novel approach allows for the use of high-quality optical measurements such as schlieren, shadowgraph, natural luminescence, and chemiluminescence that reveal previously unseen features of the detonation wave; incomplete reactant mixing produces a number of visually discernable structures. The presence and formation of detonation triple points is directly examined in a variety of reactant compositions; in some cases, the decoupling and decay of detonations occurs if an insufficient number of triple points are present. Results from these experiments are compared to a novel partial mixing model that examines a possible mechanism responsible for experimentally observed waves propagating at a deficit in comparison to the speed predicted by one-dimensional Chapman-Jouguet (CJ) theory. This work yields not only insight into the design, development, and testing of experimental RDE, but it also provides valuable test data for validating numerical simulations of RDE. More details of this work can be found in the Ph.D. thesis by Jason Burr [9]

Objectives

The primary objective of this work is to investigate the fundamental structure of the RDE combustor flowfield. The essence is to accurately identify and characterize the various features pertinent to detonation wave propagation in RDE by using a linear model combustor configuration. The model combustor allows easy visualization access, facilitating a direct study of dynamic interaction between various flow structures including shock waves, combustion zone, reactant jets, product flows, and detonation waves. Also, the model combustor allows for precise control of the initial flow conditions making it suitable to characterize the transient flowfield and various flow events such as detonation transition, quenching and reignition as a function of various propellants and flow conditions.

Experimental Setup

The linearized combustor allows for variation in the reactant composition, mixedness, and fill layer height, as well as control over pre-detonator conditions. The flexibility of the linear combustor allows for rapid testing and flowfield evaluation of numerous RDE configurations. Propagation modes for these different conditions are characterized experimentally through the identification of structures such as transverse waves, reaction zones, and triple points.

Data collected from the experimental studies of the various fuels are used to inform an analytical model of partially mixed RDE propagation. Results from the model are compared with experimental data to identify possible causes of observed detonation wave speeds. Additionally, collected data are assembled for use in future numerical validation and collaboration efforts.

The complete work include the following elements:
- Development and testing of a new novel combustor configuration that captures the essence of the RDE flowfield, neglecting curvature.
- High-quality visualizations of detonations propagating through partially-mixed and orthogonally injected reactant jets of various compositions.
- Identification of the influence of reactant mixing on the structure of detonations in RDE.
- Visualization of the reactant refresh process following a detonation transit and the role of feed plenum dynamics in this recovery.
- Investigation of detonation propagation modes for hydrocarbon mixtures with respect to transverse waves and heat release.
- A simplified analytical model of mixing limited detonation propagation and the resulting impact on detonation wave speed.

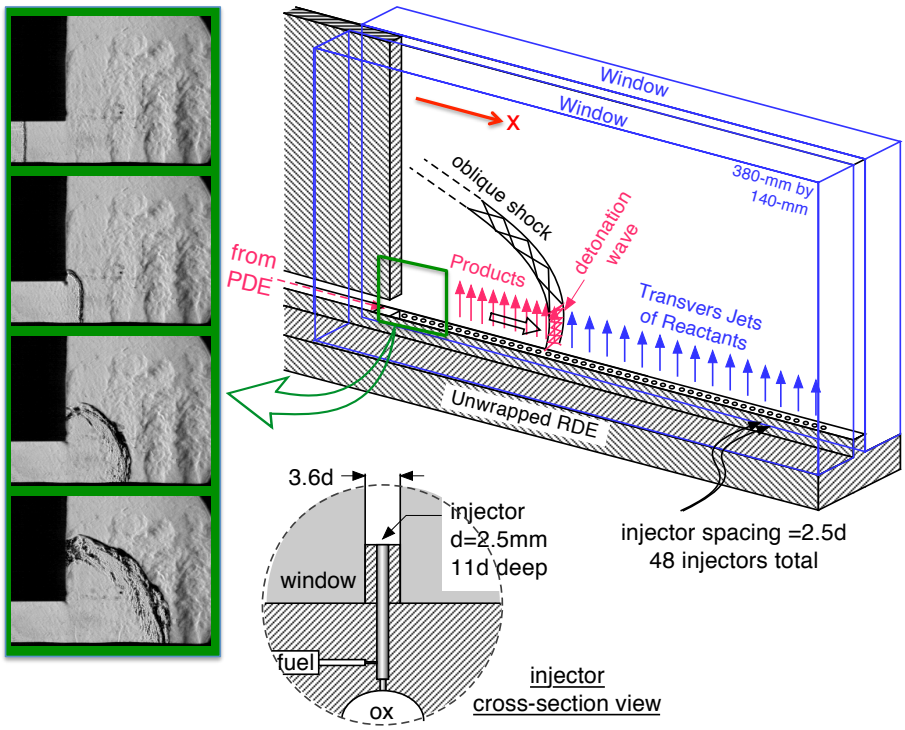

Figure 4.1. LMDE model combustor with 48 injectors

Experiments were performed in the Linear Model Detonation Engine (LMDE) combustors, shown in Fig. 4.1. The LMDE is a two-dimensional representation of an RDE with the injectors aligned linearly along a straight channel rather than in an annular channel. Under certain conditions, injection of reactants along the channel can sustain the transversely propagating detonation wave. In particular the LMDE combines attributes of the Air Force Research Lab's (AFRL) 6-inch RDE [10] and the Naval Research Lab's (NRL) premixed microinjection system [11]. Up to 48 recessed injector tubes with 1.125-inch in length and 0.10-inch diameter are used to establish premixed jets of hydrogen-air, hydrogen-oxygen, ethylene-air, ethylene-oxygen, and methane-oxygen at various composition ratios. Also, air, oxygen, or other inert gas mixtures are used as the background gas for the first cycle.

An RDE operation cycle consists of two stages (phases), with partially overlapping stages that are typically stacked in axial direction and running concurrently, as illustrated in Fig. 4.2. On one hand, the detonation transit phase starts with the arrival of a lead shock/detonation wave front, followed by associated compression, heat release and expansion processes. On the other, the injection refresh phase ends with the arrival of a lead shock/detonation wave front, preceded by fuel/oxidizer injection into transient pressure field and mixing. We have constructed two combustor models so far – one is the original model with 15 injectors, which was used to study the injection refresh phase, and the other is an extended-length model with 48 injectors, and it was used to study the detonation transit phase.

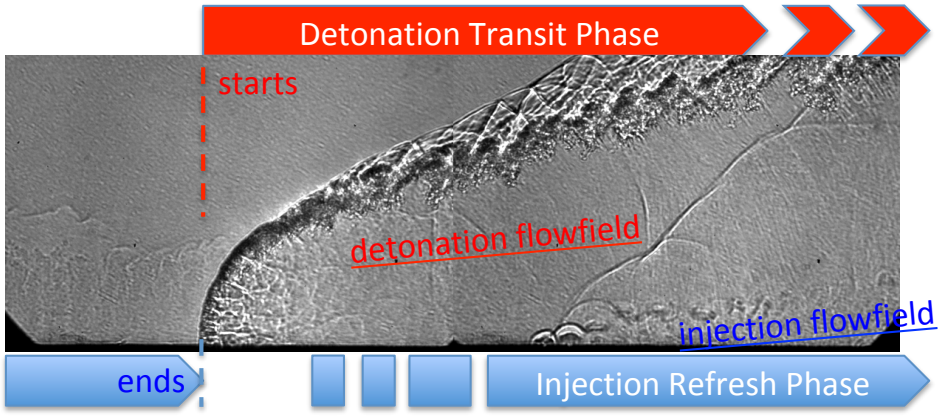

Figure 4.2. Two stages of RDE operation cycle illustrated with LMDE detonation image of CH4-O2 injection

Both shadowgraph and schlieren technique have been applied to obtain flow structure images. For analyzing the flow and acquiring the data, dynamic pressure transducers (PCB 113B24) were used in conjunction with a National Instruments cDAQ-9188. Two pressure transducers at the exit of the PDE determined the initial speed of the wave, while four other transducers mounted one-inch apart on the side metal wall tracked the transient propagation speed inside the test section. The PCB sensors have a range of ±1 kpsi and were sampled at 750 kHz. The measured values were sent via a TCP/IP connection to a desktop computer operating a LabView control panel.

4.1 Detonation Wave Characteristics Using Hydrogen As Fuel

Hydrogen-Air Detonation Wave in Unwrapped RDE Channel

Table 4.1 summarizes the flow conditions tested. The pre-detonator was operated with a stoichiometric hydrogen-oxygen mixture. The setup produced a detonation wave with relatively consistent repeatability. At the end of the pre-detonator tube, the average wave speed was measured to be 2,820 ± 70 m/s. After some preliminary experiments in which various background gases were tested, several cases including the baseline test with no transverse injection were selected for closer examination. The same conditions were used for the pre-detonator for all the cases of the jet-in-the-channel tests.

Table 4.1. Pre-detonator and Combustor Flow Conditions

	Reactants Composition	Equivalence Ratio (ϕ)	Reactant Jet Height: h_{tip} (mm)	Reactant Jet Velocity: V_{tip} (m/s)
Pre-detonator	H_2-O_2	$\phi_{mixture}$ =1.0	n/a	n/a
Case 1-B (no jets)	-	n/a	0	0
Case 2-HA (H2-air)	H_2-air	$\phi_{average}$ =0.5~1.0	25±3	52±3

When a detonation wave is formed, highly irregular and multi-dimensional structures are observed on the lead wave front. These structures were seen protruding ahead of the more two-dimensional incident shock wave surging ahead forming a leading shock wave front.

Figure 4.3 shows typical schlieren images of hydrogen-air combination, corresponding to Case 2-HA. These images revealed irregular structure for the lead wave, and showed that there were various cusps on the lead wave structure. By tracking the path of these cusps on the wave front, it seems clear that they are the triple points. The base flow visualization for Case 1-B also suggests the mechanism for triple point production. As the lead wave reflects off from the injector surface, the waves meet and create regularly spaced triple points. Although these wave interactions appear very weak in Case 1-B with no reactants, it is likely that the interactions can be stronger in the presence of combustion reaction.

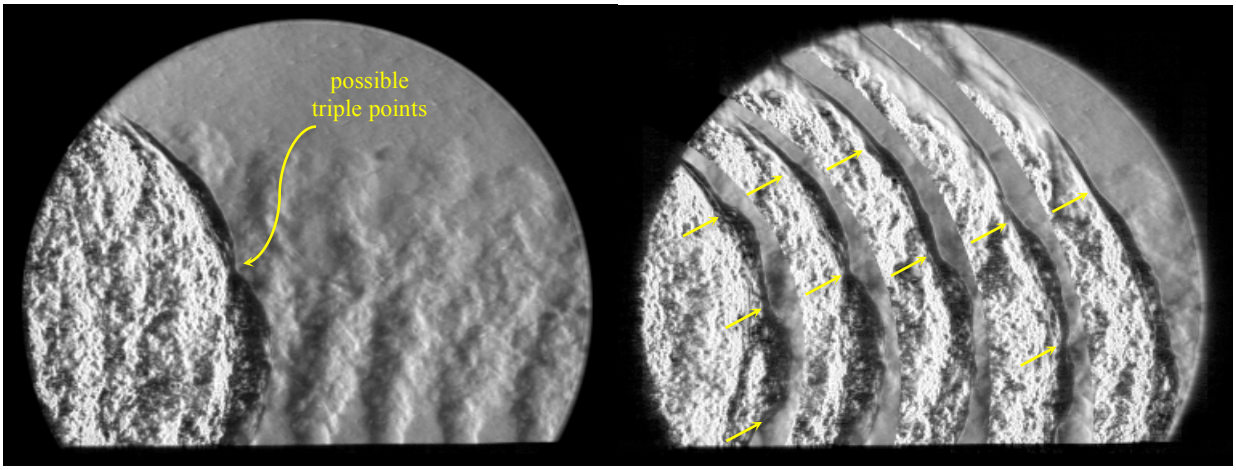

Figure 4.3. Detonation propagation into hydrogen-air mixture in Case 2-HA.
(a) evidence of possible triple point, (b) superposed image of five successive frames.

Hydrogen-Oxygen Detonation Wave in Unwrapped RDE Channel

Table 4.2 summarizes the additional flow conditions used with hydrogen-oxygen jets. Figure 4.4 shows the flowfield images for these cases taken when the respective wave is passing over the injector #13.

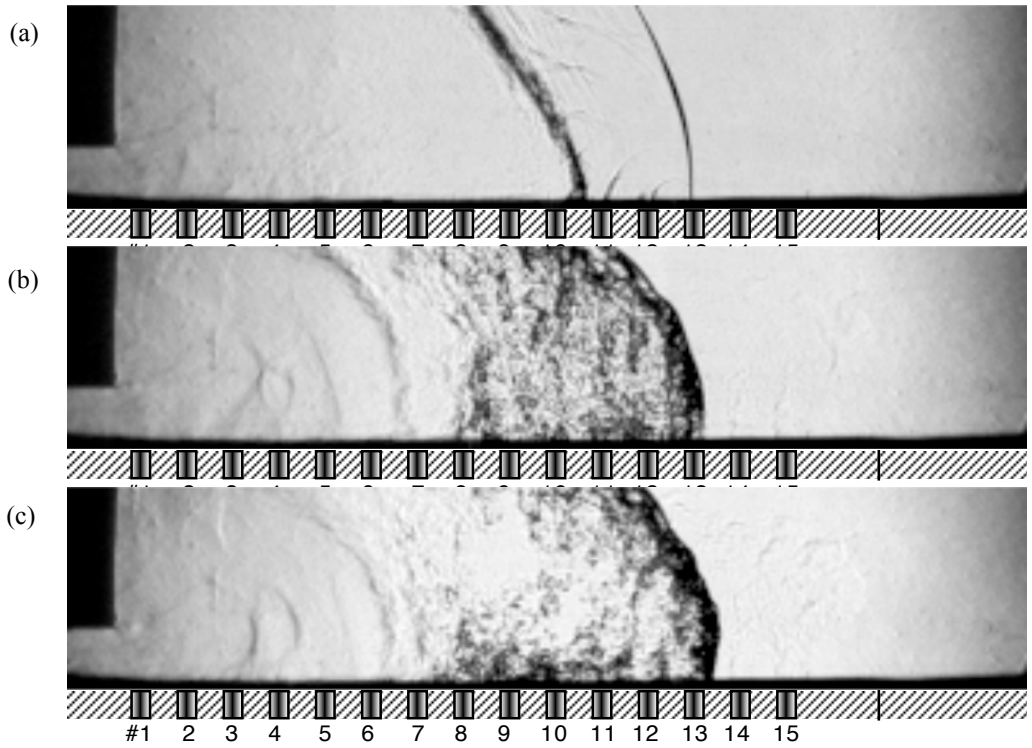

Figure 4.4. Schlieren images corresponding to (a) Case 1-B, (b) Case 3-HO, (c) Case 4-HO flowfields

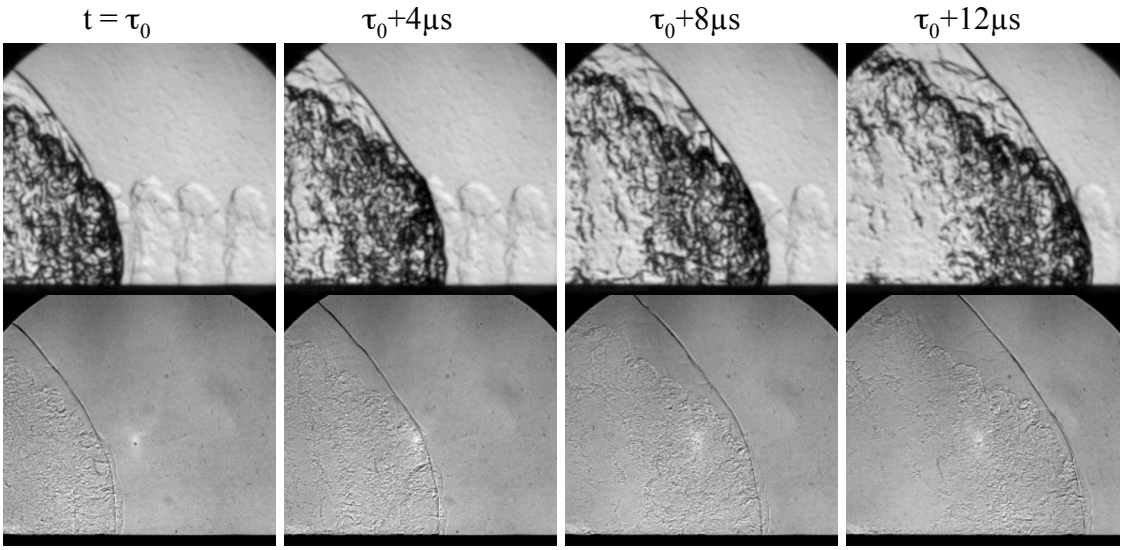

Figure 4.5. Simultaneous visualization of a detonation wave propagating across transverse jets of H_2-O_2 mixture taken at 250,000 frames per second. Top: schlieren images. Bottom: shadowgraph images

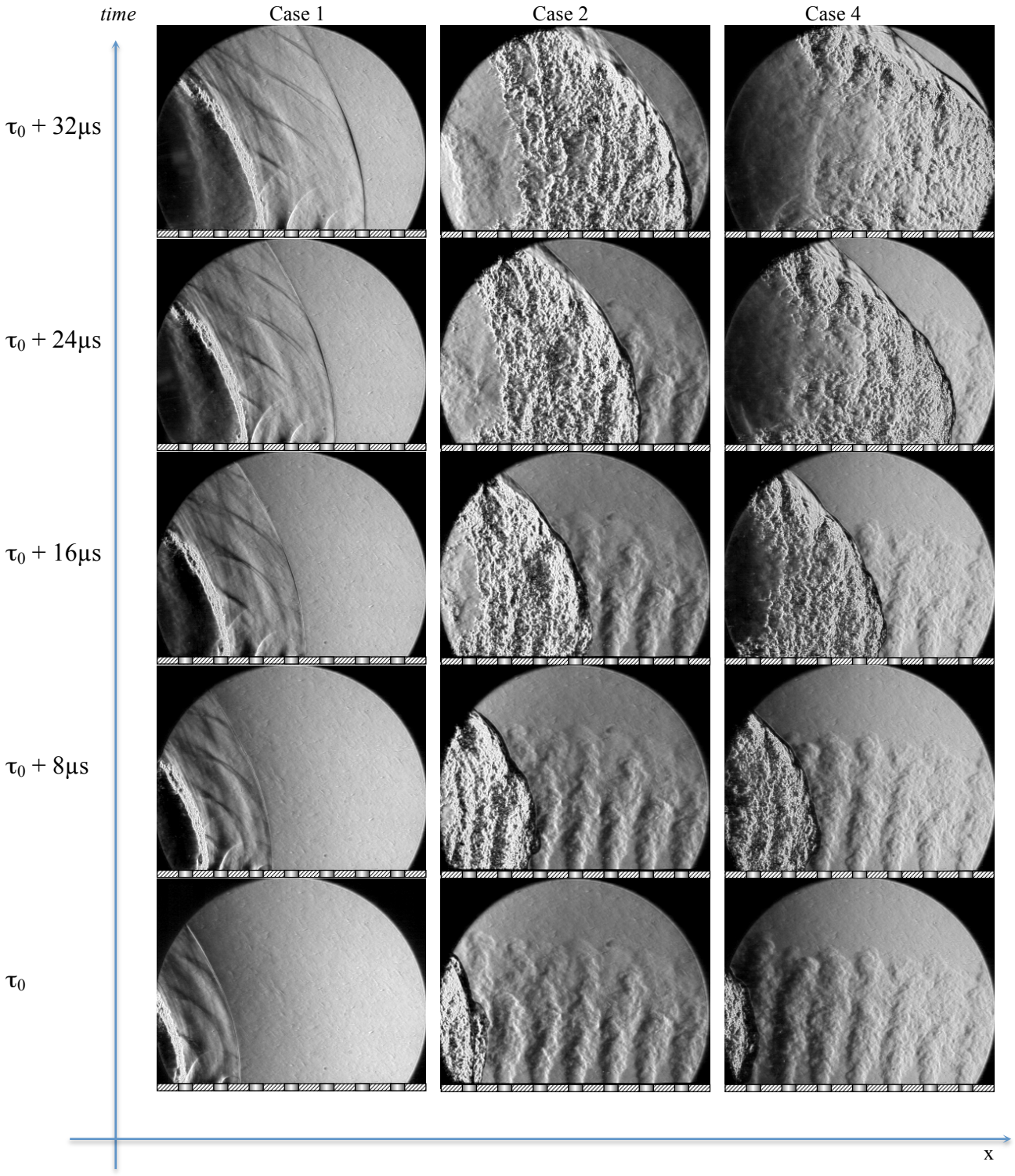

Figure 4.6. Detonation wave or blast wave propagating inside a narrow channel containing
(a) Case 1-B – no reactants
(b) Case 2-HA – hydrogen-air mixture
(c) Case 4-HO – hydrogen-oxygen mixture

Table 4.2. Reactant Jet Flow Conditions

	Reactants Composition	Equivalence Ratio (ϕ)	Reactant Jet Height: h_{tip} (mm)	Reactant Jet Velocity: V_{tip} (m/s)
Case 3-HO	H_2-O_2	$\phi_{jet\text{-}tip}$ =1.7	25±3	34±3
Case 4-HO	H_2-O_2	$\phi_{jet\text{-}tip}$ =1.4	25±3	54±3

Some of the experiments were conducted with simultaneous application of schlieren and shadowgraph visualization techniques. Figure 4.5 shows a sequence of images showing a detonation wave propagating across a row of hydrogen-oxygen reactant jets discharging from the injectors #9 through #14. They were visualized using both high-speed schlieren and high-speed shadowgraph applied simultaneously. The images show a detonation wave accelerating across the reactant jets while dragging an oblique shock through the inert gas on the background.

Figure 4.6 is a x-t representation of the detonation wave propagating in the channel with either hydrogen-oxygen or hydrogen-air being injected. Only the last 7 injectors were visualized for comparison purpose. The lead wave location can be traced to show the substantial velocity difference between these cases.

The axial velocity of the lead wave was measured using a high-speed camera, and they're plotted in Fig. 4.7. The measured values were consistent with the speed deduced from the pressure transducer data. The Case 1-B corresponds to the blast wave decay, as there is no injection of reactants into the channel. As the detonation wave enters the channel containing the background gas only, it decays into a blast wave traveling at about Mach 2. Both the Case 3-HO and Case 4-HO represent the similar composition of the reactants, containing the hydrogen-oxygen mixture. However, the injector responses for the hydrogen and oxygen feed lines were such that the partially premixed reactants did not result in uniform mixture throughout the jet. It was seen that the partial velocity of hydrogen was greater than that of the oxygen flow in some of the cases. This also affected the equivalence ratio of the mixture at the tip of the jet, which was closer to stoichiometry in Case 4-HO.

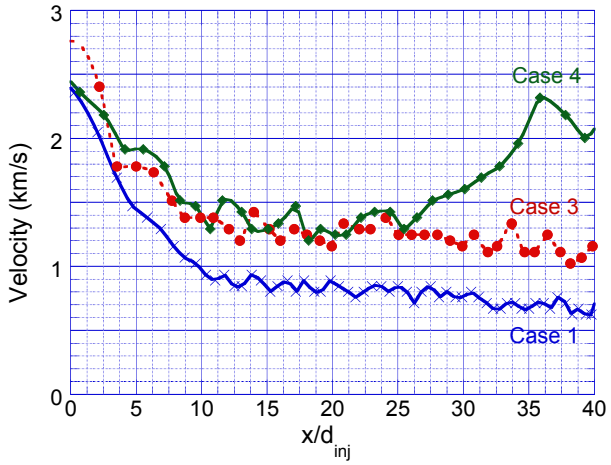

Figure 4.7. Evolution of the lead wave speed for various cases.

4.2 Ethylene-Oxygen Detonation Wave Characteristics in Unwrapped RDE Channel

Figure 4.8 shows the dynamic pressure measurements that correspond with two pre-detonator ignitions spaced 110 ms apart. For a given sensor, two distinct detonation transits are immediately identifiable as the local maxima in the signal derivative; in the case of dynamic pressure sensor #1, located 65**d** upstream of the LMDE cross-flow, the two transit times are labeled as τ_1 and τ_2 in Fig. 4.8. The resulting wave speed for a given ignition event is estimated from the delay in transit time between the two sensors and known sensor spacing. For the signals in Fig. 4.8, the first wave speed is measured as 3.0 ± 0.2 km/s, and the second wave speed is measured as 1.9 ± 0.1 km/s.

Transmission of the first detonation wave through the cross-flow is captured in Fig. 4.9. The detonation emerged from the pre-detonator and was subjected to diffraction at X = 0, then propagated through the channel at 2.4 ± 0.2 km/s.

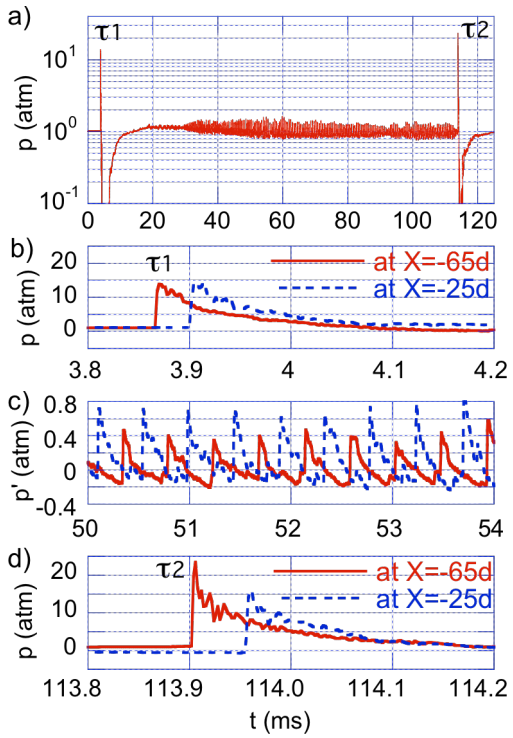

Figure 4.8. Typical recording of dynamic pressure during (a) LMDE tests of two successive detonation waves, (b) the first detonation wave transit, (c) combustion instability, and (d) the second detonation wave transit.

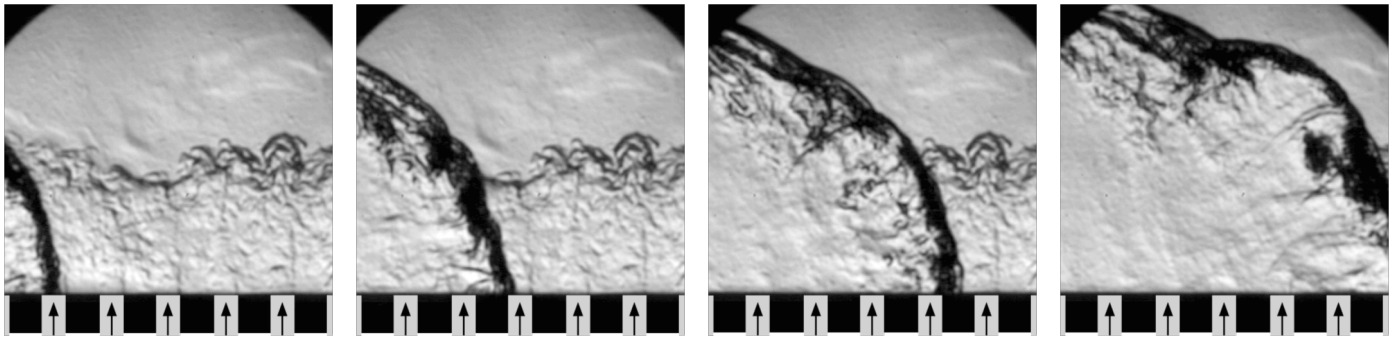

Figure 4.9. Detailed sequence of detonation wave propagating in ethylene-oxygen jets. Each successive image was taken at a 5-μs increment.

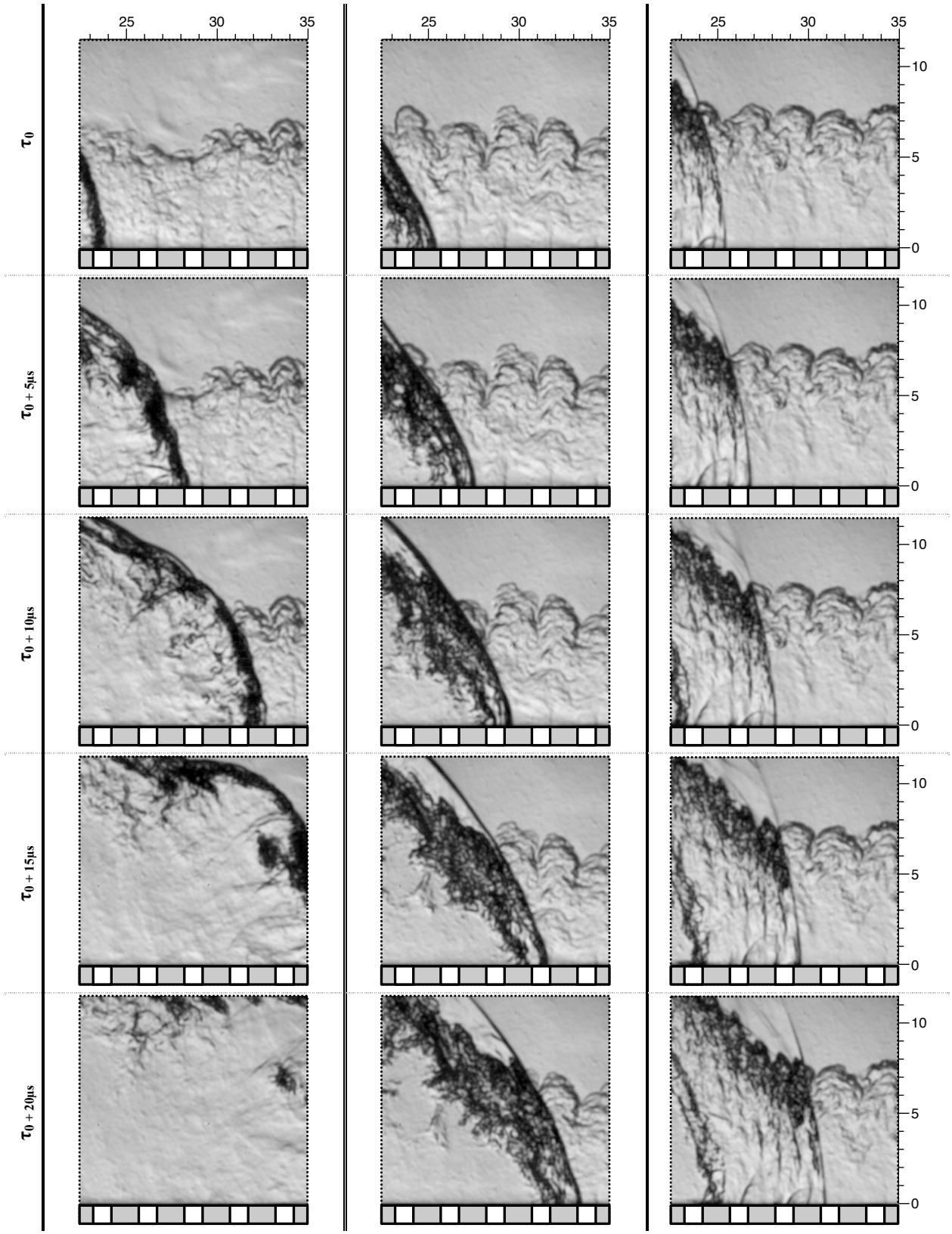

Figure 4.10. Schlieren images of detonation wave (left column), shock wave with closely coupled flame (center column), and shock wave with failed ignition (right column) propagating through ethylene-oxygen jets at various times.

Figure 4.10 shows the three observed modes of wave transit characteristics depending on the initial wave speed from the pre-detonator. Relatively low wave speed from the predetonator resulted in a non-reacting shock wave propagating at speed of 690 ± 20 m/s (right column). Although the reactant cross-flow was compressed by the shock, the only evidence of combustion in the wake of the wave was at the tips of the reactant cross-flow where the most time for mixing had occurred. Increasing the pre-detonator transmittance yielded a shock wave with a closely coupled flame structure propagating at 1030 ± 110 m/s (middle column). This mode is different from the close-coupled detonation wave, and is characterized by the stretched reaction zone and still relatively low propagation speed. Compared to the previous non-reacting mode, the increased speed of the shock further compressed the reactant cross-flow and enabled ignition of the reactant mixture. The highest wave speed case yielded a strongly-coupled detonation wave propagating at 2230 ± 80 m/s (left column).

4.3 Methane-Oxygen Detonation Wave Characteristics in Unwrapped RDE Channel

In the experiments, detonation waves were initiated via a pre-detonator positioned at the entrance of the channel combustor at appropriate timings corresponding to controlled heights of reactant jets. Amount of jet premixing was varied by independently adjusting the relative timing and flow rates of methane and oxygen. The resulting detonation wave structure was characterized for selected cases by conducting repeated experiments at each controlled condition.

In one case when the jet fill height was greater than two inches, robust detonation waves were observed consistently with strong shock-flame coupling. In other cases where the jet heights were at two inches or less, the results yielded bifurcated operational modes between detonation wave and decoupled shock-flame structure. It appears that the degree of local premixing, determined by the controlled injection timing, affected whether a detonation wave or a decoupled shock-flame structure was observed. Shadowgraph images of the detonation cases reveal the clear presence of triple points on the detonation wave front, and the results indicate that at least several triple points may be required to maintain the robustness of close shock-flame coupling and stable wave propagation in the RDE configuration.

Degree of Coupling Between Shock Wave and Combustion Zone (CH4-O2)

A large number of detonation experiments were performed in which the injection timings and the flow rates were systematically varied while keeping the equivalence ratio of the total reactants close to the stoichiometry and the reactants fill height close to a pre-selected value. To achieve this, each reactant supply pressure and the valve-open timing were independently controlled in such a way that both fuel and oxidizer jets would reach the same fill height by the time of wave arrival from the pre-detonator section.

Four selected cases are summarized in Table 4.3, which includes information on both the control settings (valve timing and fill height) and the resulting quantitative characteristics of the wave. About ten to fifteen separate runs were conducted for each case for repeatability.

Table 4.3 Injector operating conditions and the resulting flowfield and wave structure

Case	Normalized injection timing of fuel relative to oxidizer	Overall equivalence ratio	Injection fill height (h/d)	Wave velocity (m/s)	Max pressure rise (p2/p1)	Note on wave status
1-MO	0	0.8±0.2	22±3	2260±30	31±6	detonation
2a-MO	-0.3	1.2±0.2	16±2	2070±50	47±24	detonation
2b-MO	-0.3	1.2±0.2	16±2	1400±300	24±14	decoupling
3-MO	0.2	1±0.2	14±1	710±10	4.3±0.5	decoupled

The first conditions (Case 1-MO) resulted in a highly repeatable case of robust detonation wave. All of the runs in this case resulted in a clear detonation wave front with multiple triple points observed on the wave front. A shadowgraph image of a typical flowfield is shown in Fig. 4.11a, while the corresponding CH* chemiluminescence image is displayed in Fig. 4.11b. The images were simultaneously obtained, and they reveal about three to four triple points, featured on the detonation wave front. This condition results in a stable detonation wave with strongly-coupled shock wave and the flame front.

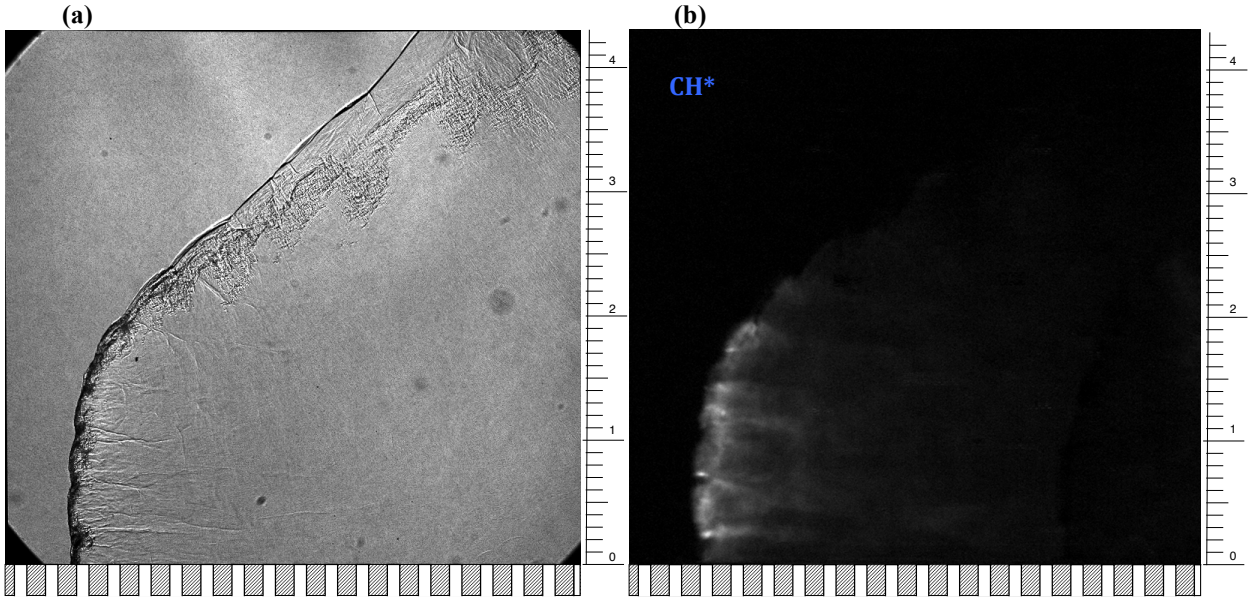

Figure 4.11 CH4-O2 detonation wave in an unwrapped RDE channel for Case 1 conditions (a) Shadowgraph, and (b) CH* chemiluminescence

Interestingly, the second conditions (Case 2-MO) produced a bifurcating set of results. During about a half of the runs (Case 2a-MO), the controlled injection setting resulted in a strongly-coupled wave front similar to the Case 1-MO. However, during the other half of the runs (Case 2b-MO), the same condition setting resulted in a much weaker coupling between the lead shock wave and the flame front. As a result, a decoupling shock-flame structure was observed for Case 2b-MO. Typical shadowgraph images for these two cases are shown in Fig. 4.12.

In Case 2a-MO, some triple points are visible on the wave front, whereas in Case 2b-MO, the shock wave and the flames are starting to decouple and no triple point is visible. Also, there are substantial differences in these two cases for the wave propagation speed and the maximum pressure rise. Both the observed wave velocity and the maximum pressure rise are much higher for Case 2a-MO.

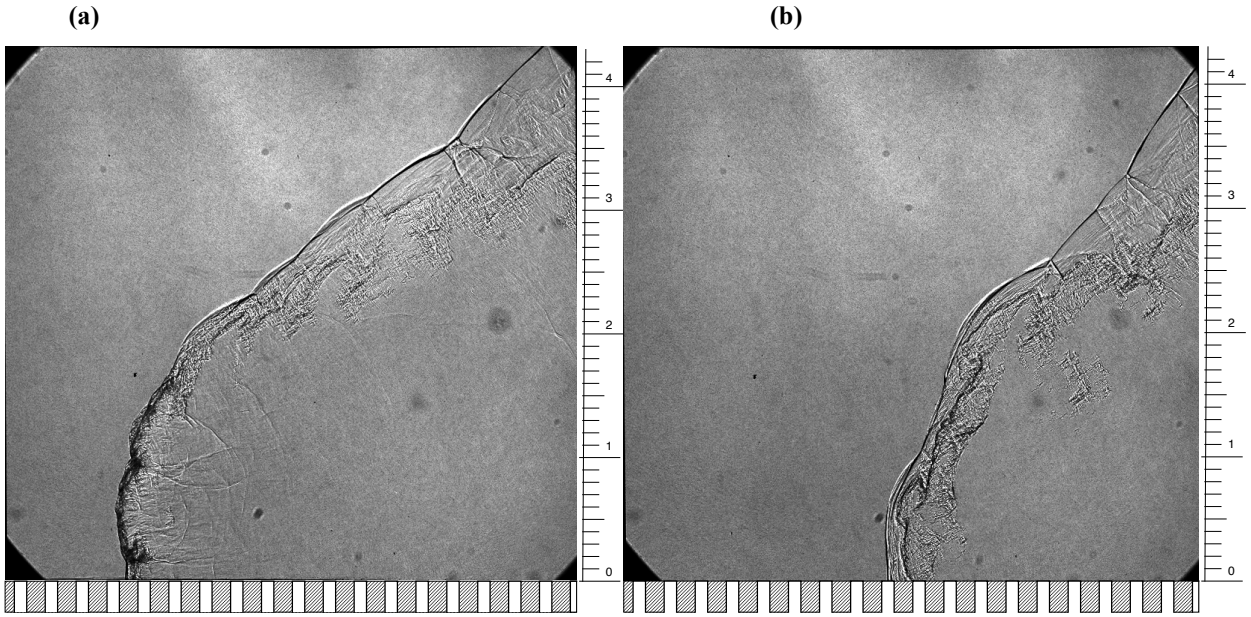

Figure 4.12 CH4-O2 detonation wave in an unwrapped RDE channel for Case 2-MO conditions (a) Case 2a-MO with strongly-coupled wave front, and (b) Case 2b-MO with decoupling detonation wave

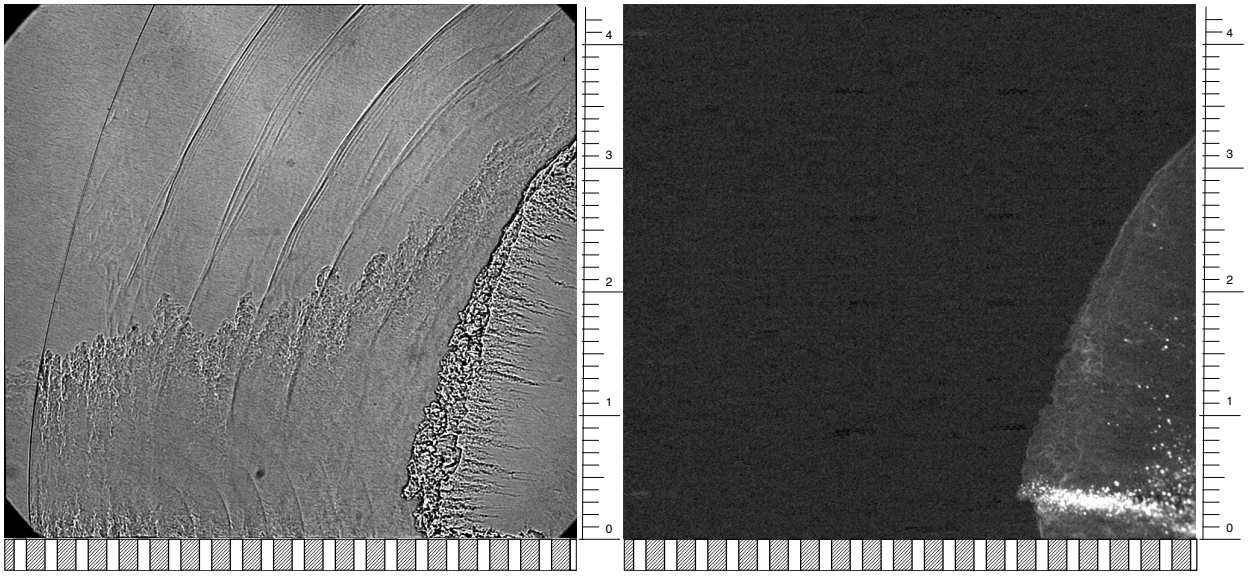

Figure 4.13 CH4-O2 decoupled detonation wave in an unwrapped RDE channel for Case 3-MO conditions (a) Shadowgraph, and (b) flame luminosity image

Figure 4.13 represents the last conditions (Case 3-MO) that produced another set of highly repeatable results, where the lead shock wave was always observed in a decoupled state with the flame fronts. The flame fronts in this case trailed the lead shock by a substantial distance (2.5~3 inch). This situation should be unstable, as temporarily increasing the separation distance would accelerate the decoupling process while decreasing it would lead to the deflagration-to-detonation transition process. Thus, maintaining such a large separation distance could not be sustainable in a single wave situation. Nevertheless, it might be possible to have a periodic situation in a round annulus if there were multiple waves with periodic re-ignition and decoupling processes or multiple waves with a steady separation being reinforced by system acoustic excitation (i.e., tangential-mode combustion instability). In the latter scenario, acoustic coupling between pressure pulses and heat release oscillations would sustain the proper separation between the lead wave (the main source of pressure oscillations) and the flame front (heat release oscillations).

Detonation Wave Speed on Reactant Fill Height and Mixing

The three sets of operating conditions – injection timings and fill heights – presented in the previous section resulted in (i) Case 1-MO with strongly-coupled detonation wave, (ii) Case 2-MO with marginally-coupled or decoupling waves, and (iii) Case 3-MO with totally decoupled shock and flame fronts. While the final results on the wave characteristics seemed to be clearly dependent on the initial state of reactants mixing, it is difficult to quantify the degree of premixing in these experiments. Nevertheless, it is expected that the mixing will likely depend on the fill height in an evolving jet, almost impulsively started.

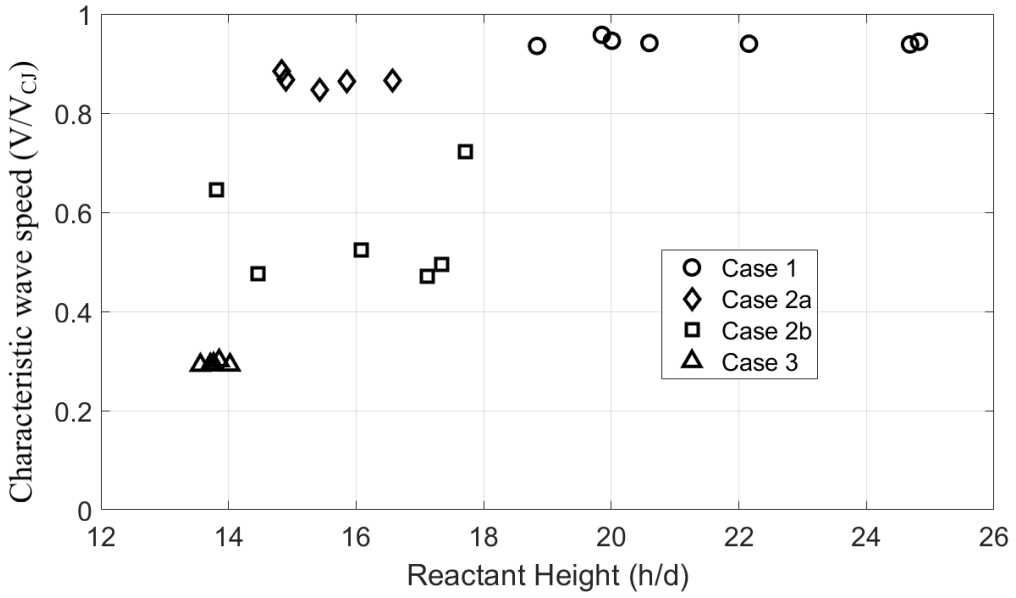

Figure 4.14 A plot of the lead wave speed .vs. CH4-O2 reactant fill height in an unwrapped RDE channel

In Fig. 4.14, the measured wave speed is plotted against the measured fill height for all the runs from those cases presented previously. In this plot, the wave speed is normalized with the 1-D Chapman-Jouguet (CJ) speed, while the fill height is normalized with the injector diameter of 0.1-inch. The results suggest that when the fill height was above 1.9 inch, all of the runs

produced the wave speed very close to the 1-D CJ speed. The reactant fill height between 1.4 and 1.8 inch resulted in a marginally-coupled detonation wave with scatted wave speed. Finally, the fill height below 1.4 inch resulted in a clearly decoupled wave, with the lead shock propagating significantly ahead of the ensuing flames.

Another plot in Fig. 4.15 shows the measured wave speed correlated with the calculated heat release fraction, that supports the detonation wave. Then, the heat release fraction would be related to the mixed reactants fraction that releases heat via the detonation mode. Again, the correlation results seem to support the following conclusions:

- Case 1-MO with the relatively high reactant fill height resulted in the greater heat release amount in the detonation mode. This resulted in the faster detonation wave speed close to the CJ speed.
- Case 3-MO with the relatively low reactant fill height resulted in poor premixing, low amount of heat release in the detonation mode, and hence slow wave speed.
- For the fill heights between the above two critical cases, the results are scattered among closely-coupled detonation waves (Case 2a-MO) to decoupling detonation waves (Case 2b-MO).

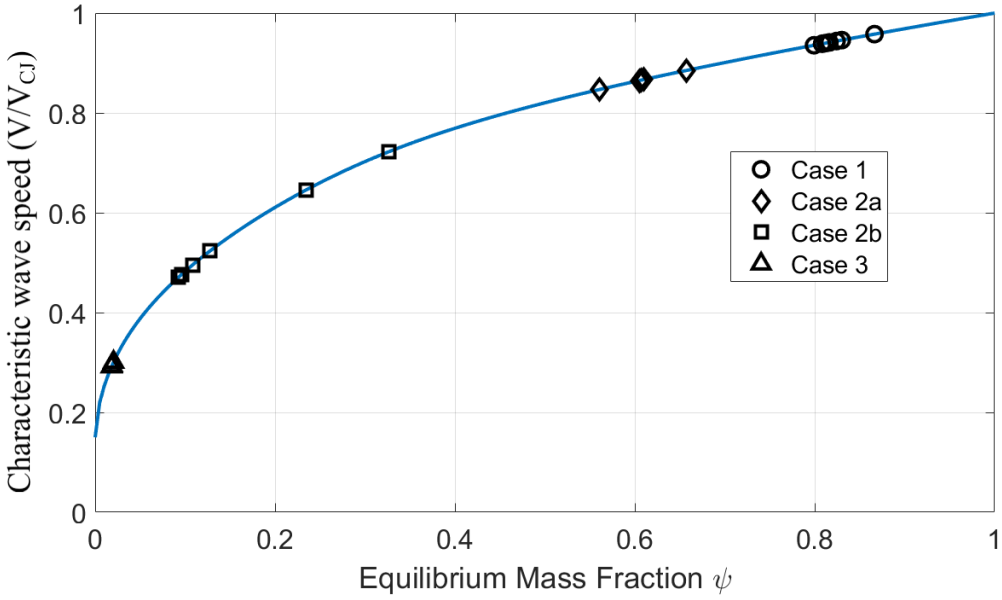

Figure 4.15. A plot of the lead wave speed .vs. CH4-O2 mixture fraction that supports the detonation wave

5.0 Interaction of Detonation Wave and Injector Flowfield

Objectives

The objectives are (1) to better understand the interaction between detonation wave and the injector flowfield, (2) to characterize the injection refresh behavior as a function of both the combustor wave dynamics and the injector geometry, and (3) to quantify the refresh characteristic delay time with respect to the wave strength and multi-wave interaction inside the combustor.

Experimental Setup

Two different experimental setups are used for this study.

One setup uses a simple rectangular detonation tunnel fitted with an isolated model injector. The schematic of the setup is shown in Fig. 5.1. Two different injector types have been tested: one is an impinging-type injector shown in Fig. 5.1, while the other is a recessed tube injector described previously. Detonation wave-injector flowfield interaction experiments are carried out while testing these injectors. Typically, the background gas for detonation wave uses a stoichiometric mixture of either a pure hydrogen-oxygen mixture or that diluted with inert gases.

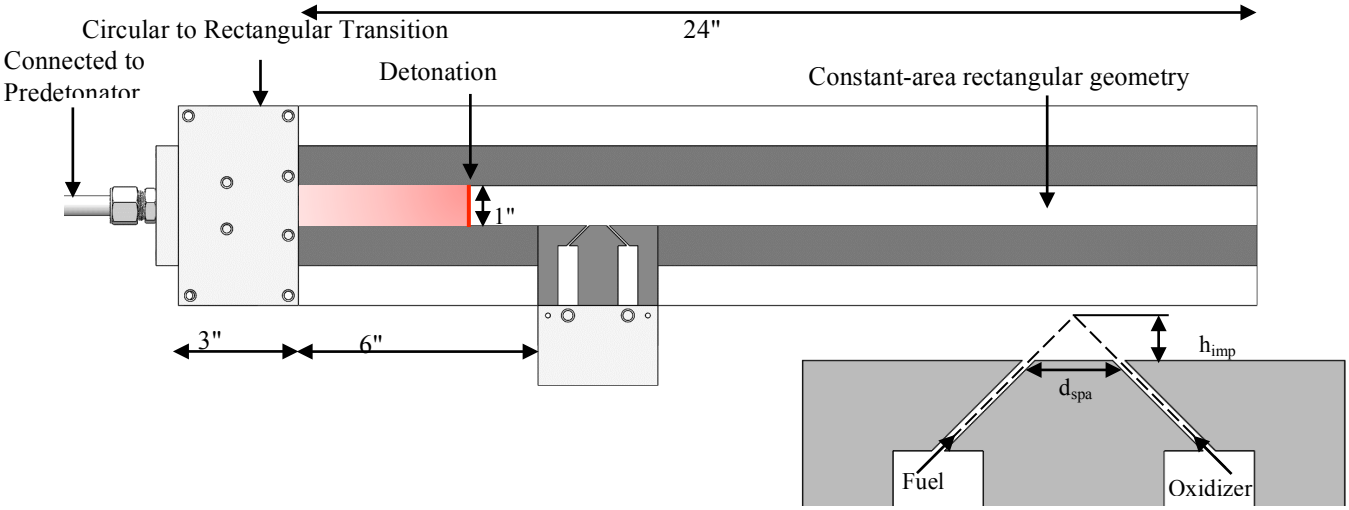

Figure 5.1: Schematic of detonation tunnel and model injector

The various flow conditions associated with the injector flowfield are created by varying the stagnation pressure of the reactants to adjust the net mass flow rate and the initial height of the injected flowfield.

The other setup uses the LMDE combustor – the unwrapped RDE configuration introduced in the previous section. The injector is a recessed tube with a depth-to-diameter ratio of 11, and it is connected to the fuel and oxidizer lines near its base

5.1 Effects of Mixing and Combustion; due to detonation wave-injector flowfield interaction (from Shikha Redhal's MS scholarly paper, 2019)

Transient interaction between a propellant jet flowfield and a propagating detonation wave is studied experimentally, using a rectangular detonation tunnel with an isolated model injector mounted on one side. The study is motivated by the desire to understand the effects of various fuel-oxidizer mixing patterns on the detonation wave propagation in RDE combustor. A parametric study is conducted with two different injector types – one, using an unlike-impinging doublet injector, and the other, a recessed partially-premixed jet injector, and also by varying the degree of mixing via timing control of the fuel and oxidizer injection. It is shown that under certain conditions a zone of poor mixing or improper mixture can affect the detonation wave propagation by causing a locally distorted wave front. Depending on the wave strength and the degree of mixing, three different types of wave response are observed – 1) relatively little or no effect on the wave propagation possibly due to rapid mixing of the propellants, 2) local de-coupling of shock and flames, followed by subsequent quenching of detonation wave, due to poor mixing, and 3) re-ignition after a short induction delay due to partially premixed reactants. The interaction leads to different detonation wave characteristics as well as different average wave speed in the RDE. It is also shown that the re-ignition of detonation wave can generate a reverse propagating wave. These processes can explain the variations in the wave speeds and show the detonation wave decoupling and re-ignition under different conditions. It can be further concluded that these interactions can play an important role in the design of the injectors for the RDEs.

5.1.1 Wave-Flowfield Interaction with an Impinging Type Injector

The state of the reactant mixing and the jet penetration height affected the wave propagation characteristics in the channel. Possible quenching and reignition processes are also observed and discussed. There were roughly three different types of interactions observed. In the first type, the detonation wave propagates through the reactant flowfield with relatively little interaction. In the second type, the detonation wave appears to be quenched propagating through a poorly mixed area, and any possible reignition is not immediate. In the third type, the detonation wave appears to start a decoupling process briefly but the shock-enhanced mixture reignites the detonation wave in a relatively short time later, starting reverse propagating pressure waves. These three types are summarized in Figs. 5.2, 5.3, and 5.4.

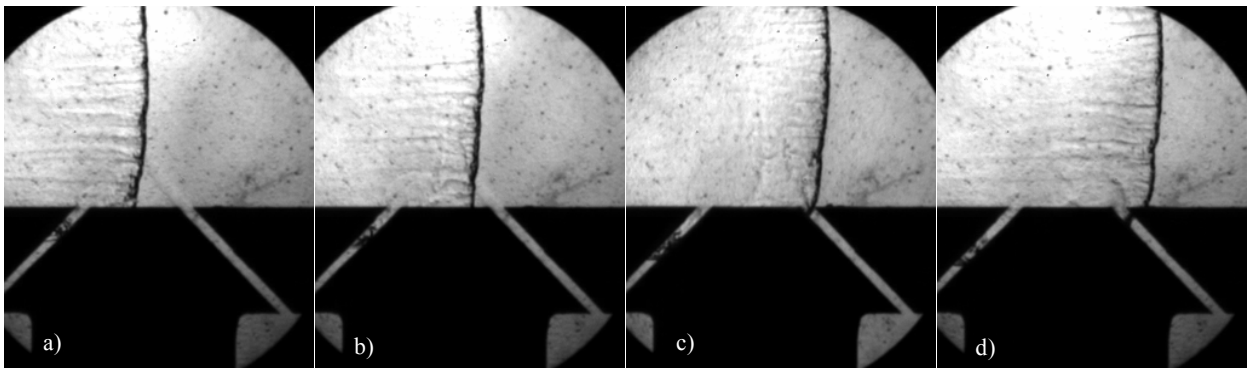

Figure 5.2. Very little interaction (Type A) between detonation wave and the injector flowfield, resulting in relatively smooth transition

In Fig. 5.5, the last type of interaction is elaborated with 3-μs interval images showing the detonation wave going through a brief decoupling and then recovering via reignition process.

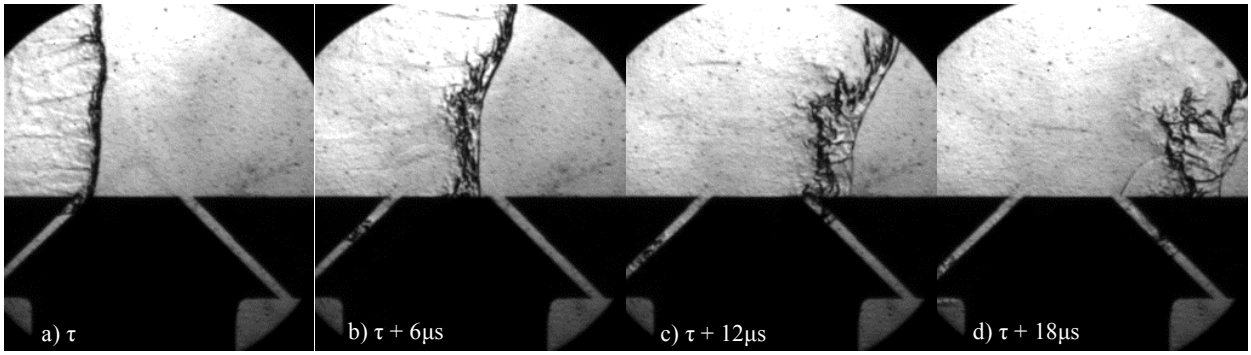

Figure 5.3. Type B interaction between detonation wave and the injector flowfield, resulting in local wave quenching or decoupling of shock and flame

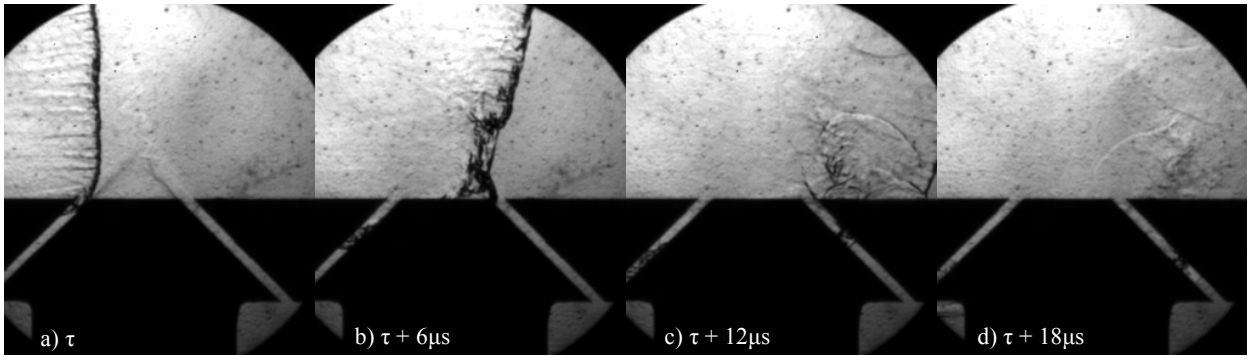

Figure 5.4. Type C interaction between detonation wave and the injector flowfield, resulting in brief local quenching followed by immediate reignition

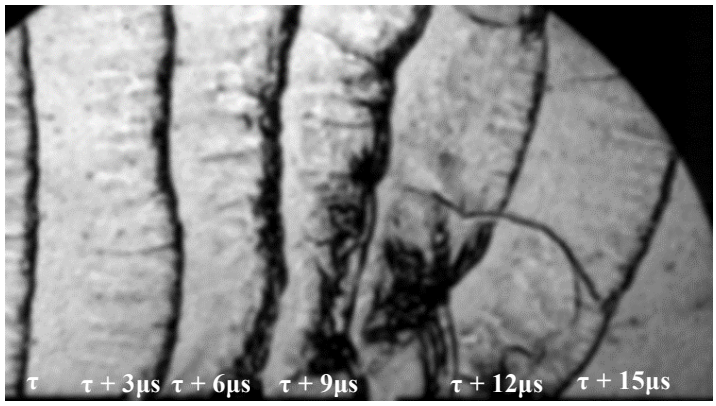

Figure 5.5. A sequence of brief quenching and reignition in Type C interaction

5.1.2 Onset of Counter-Propagating Wave

The process of local quenching and reignition can produce a strong pressure disturbance in the flowfield, enough to produce a blast wave. One such sequence is described in Fig. 5.6, where an initial decoupling of the detonation wave produces a pocket of unreacted mixture, which later

ignites producing a backward-propagating blast wave. Such a wave propagating in the opposite direction from the original detonation wave direction could be a source of counter-rotating detonation wave if the conditions were right for fresh mixture reignition.

(i) decoupling of the lead shock wave and the flame front as the detonation wave passes over a poorly mixed zone

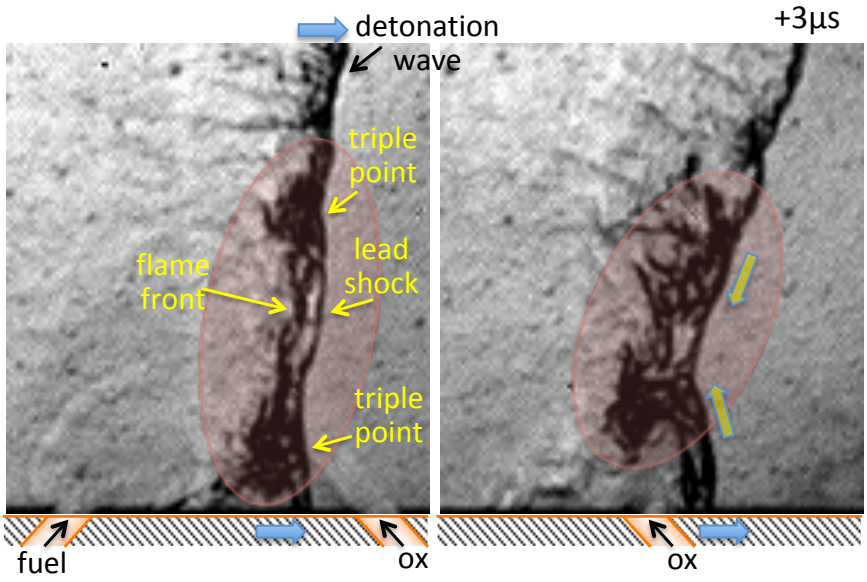

(ii) merging of the triple points toward the separated zone of unreacted mixture trapped between the lead shock and flame front

(iii) ignition and sudden reaction of the trapped mixture setting up a "micro-explosion"

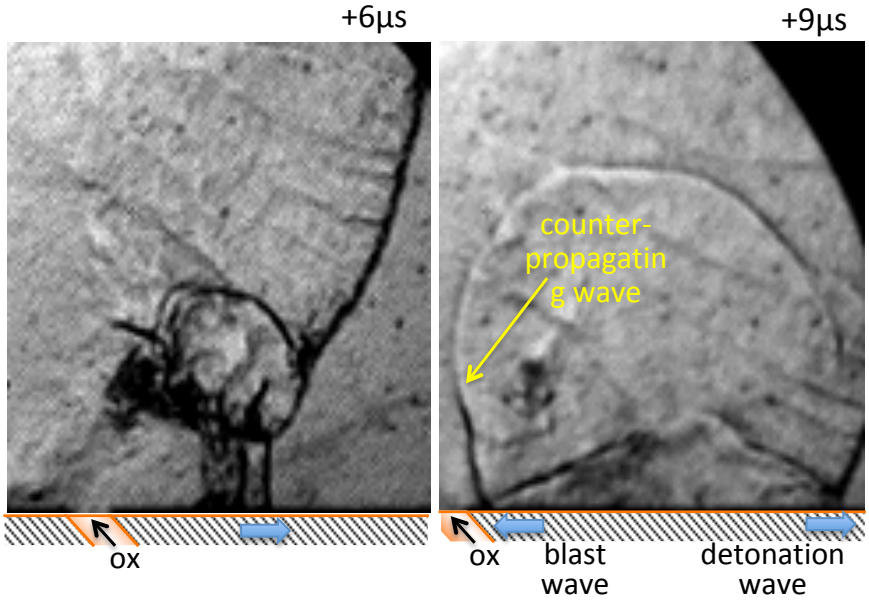

(iv) re-establishment of the detonation wave front in the original direction and onset of the counter-propagating blast wave

Figure 5.6. A sequence of shadowgraph images showing onset of counter-propagating wave

More details of this work can be found in the M.S. scholarly paper by Shikha Redhal [12]

5.2 Effects on Injection Refresh Dynamics; due to detonation wave-injector flowfield interaction (from Minwook Chang's paper, 2020)

Inside a rotating detonation engine (RDE) combustor, a sudden pressure jump associated with each detonation wave suppresses reactant jets periodically. Refresh jets of reactants appear in the combustor after a characteristic delay time that depends on the RDE operating condition. In this investigation, the characteristic response of refresh jets is experimentally investigated using a linear channel combustor, which was designed to simulate an unwrapped RDE combustor. The strength of the waves is controlled using a pair of pulse detonation engine (PDE) tubes and adjusting their mixture composition. The PDE tubes set up detonation waves that propagate over the surrogate reactant jets in the linear channel combustor. At first, nitrogen gas was used as surrogate reactants creating non-reacting refresh jets, which interacted with blast waves, now decoupled from the original detonation waves. The jet refresh behaviors including the characteristic delay time and the initial velocity at the onset of refresh were experimentally measured as a function of wave strength, wave interaction, and refresh jet flow rate. When interacting with a single wave, refresh jets follow a well-behaved growth pattern, with the refresh delay time proportional to the wave strength and inversely proportional to the jet flow rate. However, when two waves collide and interact inside the channel, the refresh jets exhibit more complicated recovery behavior. More specifically, the refresh jet closest to the point of wave collision recovers first, followed by other refresh jets closer to the point of collision and depending on each wave speed. The refresh jet results are reported as a function of the control parameters. It is expected that they provide an enhanced understanding of the physical processes inside an RDE combustor, especially during a slapping-mode operation. [13]

Experimental Setup

In this investigation, the LMDE combustor described in the previous section is used. Among the 48 injectors lining the linear channel, only eight adjacent injectors in the middle are utilized for refresh behavior investigation. Inert gas such as nitrogen is discharged through those eight injectors. The nitrogen jets from the middle eight injectors are subjected to the detonation waves that approach the set of injectors from each side.

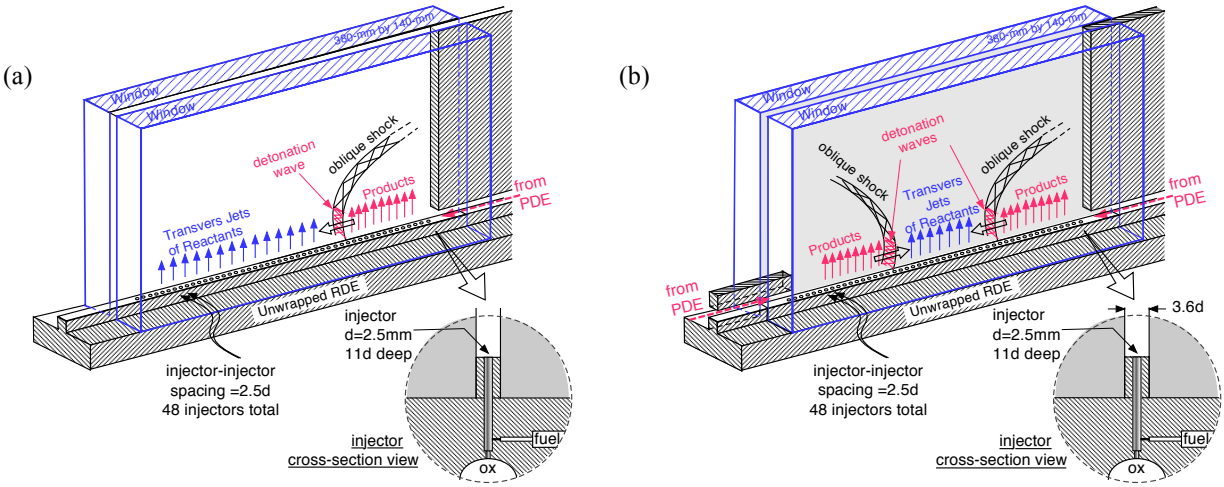

Figure 5.7 Experimental setup to study interaction between detonation wave and injection refresh dynamics (a) single-wave mode, and (b) slapping-wave mode

Two different boundary conditions are tested in this experiment, and they are illustrated in Fig. 5.7. On one hand, Fig. 5.7(a) represents a normal operating condition with a single wave propagating over the injectors. On the other hand, Fig. 5.7(b) corresponds to an experiment with counter-rotating waves similar to the slapping-mode operation. At each end of the channel, a PDE tube or a pre-detonator generates a detonation wave that propagates into the pre-established injector jets. The pre-detonators used various combinations of hydrogen-oxygen mixture and timing-controlled ignition to obtain different wave velocities. The initial and background conditions are summarized in Table 5.1 for those experiments, where conditions for (i) a single wave running from right to left, or (ii) two counter-propagating waves running in both directions are simulated.

Table 5.1. Experimental setup operating conditions

Reference Test #		Injector Conditions		Combustor Conditions	
		Plenum-Jet Pressure Ratio, P_0/P_{jet}	**Average Jet Velocity, V_{inj} [m/s]**	**Pressure Gain Ratio, P_2/P_1**	**Local Wave Velocity, D_{wave} [m/s]**
Single Wave	Case 1-N	2.2	89	4.1	674 ± 30
	Case 2-N	4.1	180	4.5	708 ± 30
	Case 3-N	6.2	290	4.6	717 ± 30
	Case 4-N	8.0	360	6.6	851 ± 30
Counter Waves	Case 5-N	2.4	98	6.4~18	840 ± 30 (LR) 1400 ± 30 (RR)

Pressure measurements using two additional pressure transducers mounted inside a pre-detonator tube are used to obtain more information about the initial wave strength entering the test section. Figure 5.8 shows a pressure-time trace associated with these measurements during a typical testing operation.

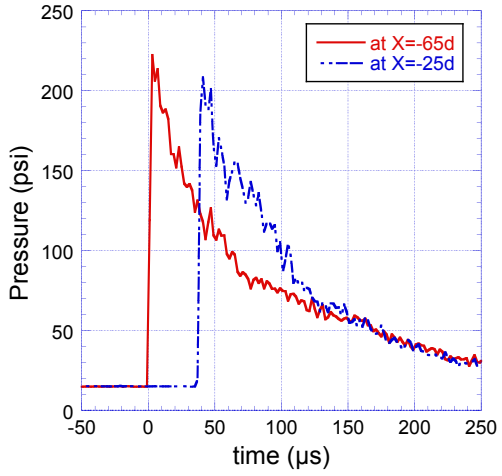

Fig. 5.8. Pressure-time traces associated with a typical detonation wave before it enters the test section

Experiments are performed with a single-wave case with and without the refresh jets. The pressure data obtained from the four pressure transducers mounted along the combustor wall are presented in Fig. 5.9. As the detonation wave enters the test section and propagates along the channel which is deprived of the reactants, the wave decays into a blast wave and the strength weakens. The measurements with non-reacting jets indicate that peak pressures at x2, x3, and x4 are somewhat lower than the case without the refresh jets. A possible reason for this behavior is the entrainment effect caused by the transversely flowing jets. Other than this, there is no significant difference between the different mass flow rate cases. These pressure measurements represent the injector exit conditions after the wave passage over the injector flow-field.

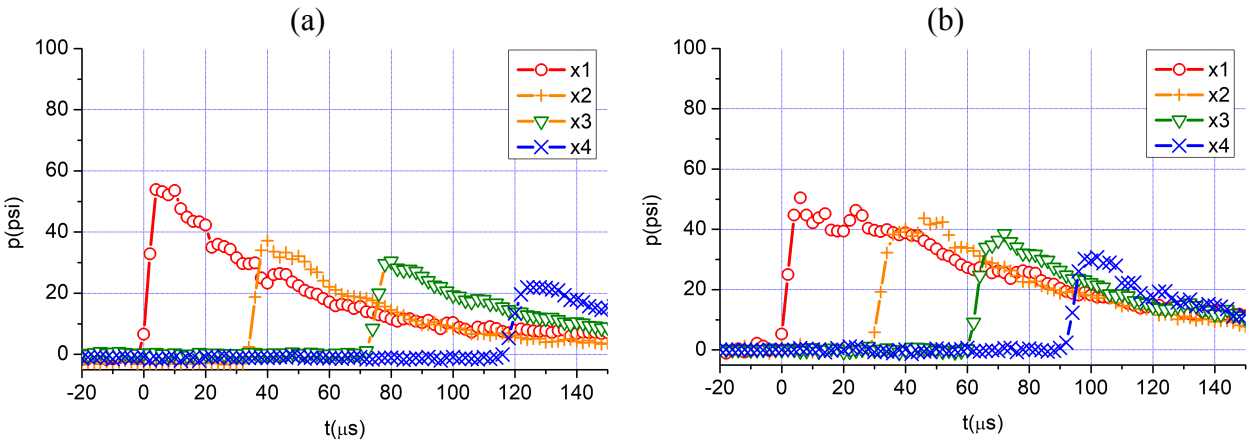

Fig. 5.9 Pressure measurements for single-wave cases (a) with and (b) without the refresh jets

Also, high-speed schlieren visualization was applied for these investigations. The results were used to obtain quantitative information regarding the refresh jet characteristics. Fig. 5.10 represents a composite image showing the development of the refresh jet over the injector #1. Recovery behaviors of various refresh jets following each imposed wave passage are shown for four different mass flow rates in Fig. 5.10 (a)-(d). Figure 5.10 (a) shows the injection refresh of the lowest mass flow rate case. It takes a relatively long delay time to establish the similar jet height in comparison to other cases. Following the establishment of the first refresh jet front, there is a subsequent refresh jet front developing after a time delay suggesting jet oscillations. It can be seen that the characteristic time difference between the first and second delays is a little more than 200 μs in this case.

For Case 2-N results with a higher mass flow rate, refresh jet oscillation behavior is not as obvious as in Case 1-N. This implies that there is a bit more damping in this case with a greater mass flow to overcome the exit pressure. Nonetheless, the first injection refresh time delay remains roughly identical to that from the Case 1-N. For Case 3-N, the ensuing flow-field appears to be significantly different from those in Cases 1-N and 2-N. For both Cases 3-N and 4-N with higher mass flow rates, the refresh jets not only rebound more quickly with a shorter delay time but the jets grow faster inside the combustor.

From the high-speed schlieren images, the jet front's height is measured for the first three injectors. The data for the growing refresh jets for Case 1-N is deduced from the schlieren images and plotted in Fig. 5.11. The refresh jet first appears after a delay time of about 130-150

μs, followed by the second refresh front at about 200 μs later from the first refresh. Various delay times and initial velocity information for the first three injector jets are summarized in Table 5.2.

Fig. 5.12 shows the growth of the refresh jets for Case 4. The refresh jet first appears after a time delay of about 80-150 μs. Interestingly, there seem to be two different velocities associated with refresh jet fronts. The first one appears to be a slower jet just overcoming the high pressure at the jet exit, while the second refresh with a faster velocity seems to be similar in characteristic with the other cases. The measured time delay data and the initial velocity data for the Case4 are reported in Table 5.3.

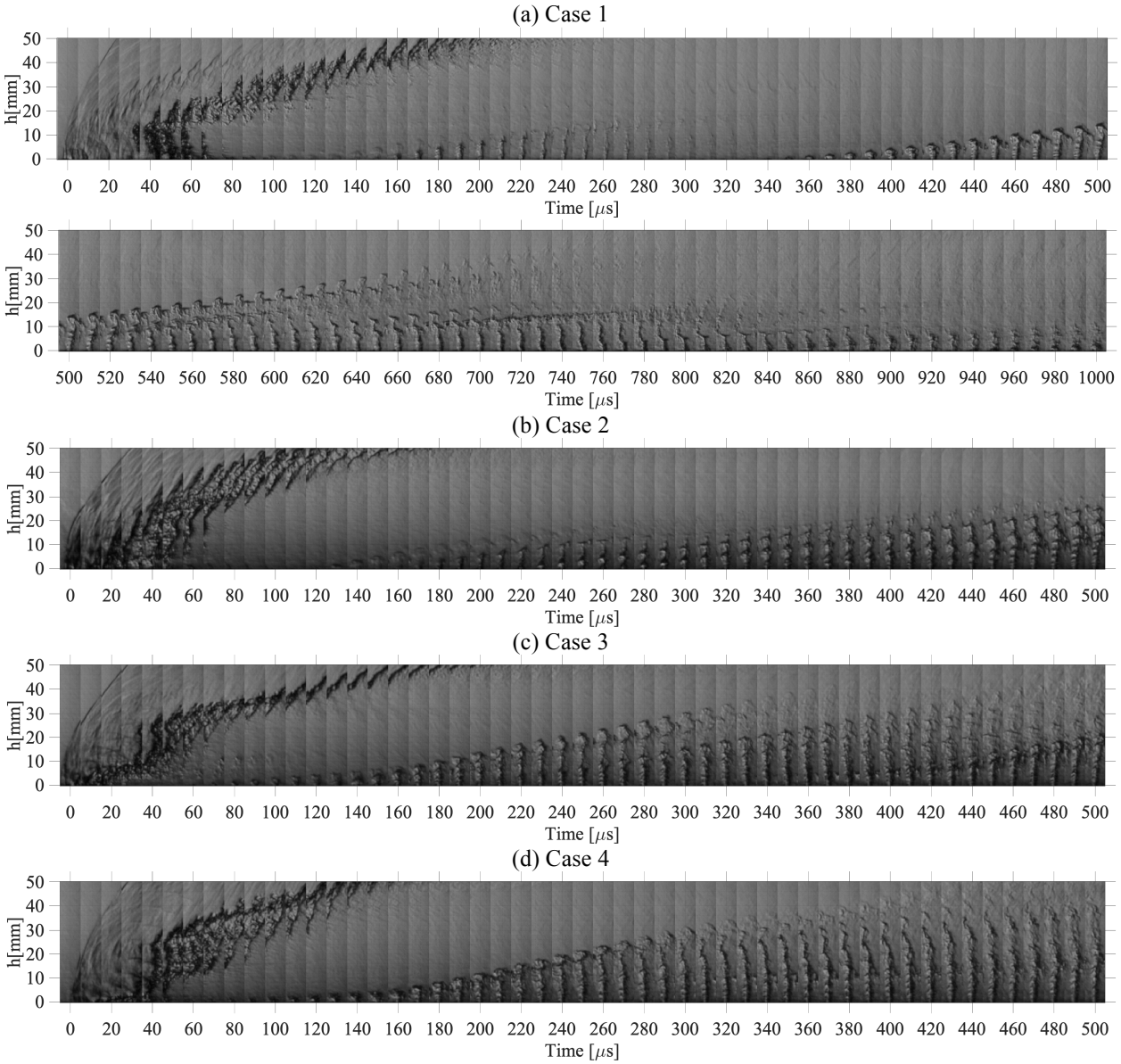

Fig. 5.10 Composite images showing the onset and growth of the refresh jet from injector #1 following the wave passage for (a) Case 1, (b) Case 2, (c) Case 3, and (d) Case 4

For all of the cases considered, there seems to be one common characteristic time delay around 140±10 μs. As the mass flow rate increases, however, the refresh jets may recover sooner if its stagnation pressure can overcome the combustor pressure. Such delay time depends on the average jet flow rate, which is related to its stagnation pressure. In other words, for a higher mass flow rate case, jet stagnation pressure can shorten the refresh time delay by overcoming the injector exit pressure.

Table 5.2. Characteristic time delays and initial velocities of refresh jets for Case1 conditions

	τ_{delay} (μs)	V_1 (m/s)	τ_{delay} (μs)	V_2 (m/s)
Inj #1	151.3	135.7	353.4	90.8
Inj #2	129.4	139.2	349.0	73.5
Inj #3	134.4	141.4	-	-
Avg.	**138 ±9**	**139 ±3**	**351**	**82**

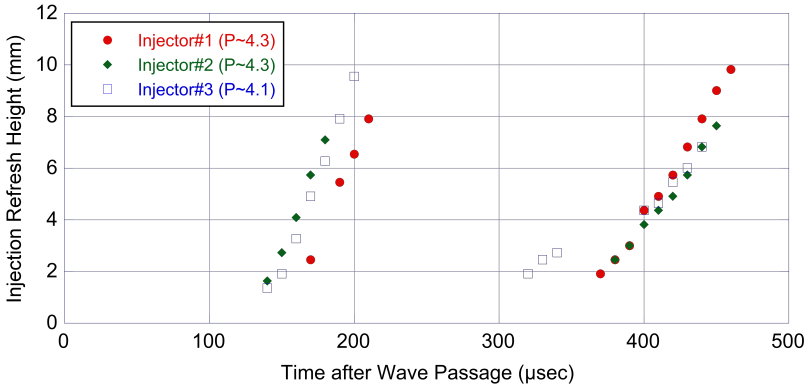

Fig. 5.11. Growth of refresh jets for Case 1-N conditions

Table 5.3. Characteristic time delays and initial velocities of refresh jets for Case4 conditions

	τ_{delay} (μs)	V_1 (m/s)	τ_{delay} (μs)	V_2 (m/s)
Inj #1	80.9	63.2	143.7	188.3
Inj #2	74.8	57.0	146.5	186.1
Inj #3	96.2	88.0	148.5	207.9
Avg.	**84 ±9**	**69 ±13**	**146 ±2**	**194 ±10**

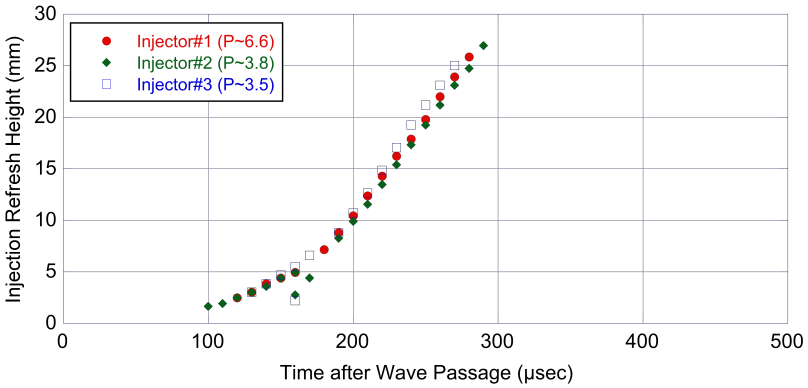

Fig. 5.12. Growth of refresh jets for Case 4 conditions

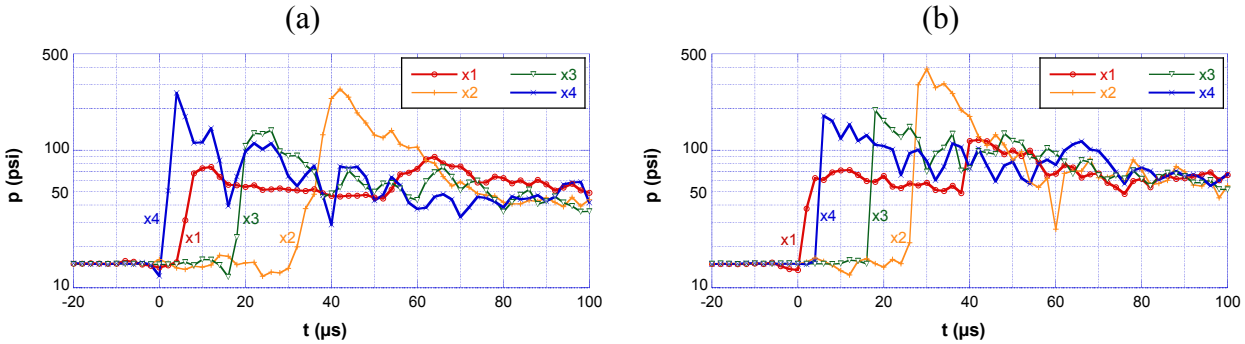

Fig. 5.13. Pressure measurements for two-wave cases (a) with and (b) without the refresh jets

Fig. 5.13 shows the pressure-time traces associated with the counter-propagating two-wave cases. Similar to the single-wave cases, the pressure amplitude is higher without the refresh jets than with the jets. Fig. 5.13(a) shows that the right-running wave enters the injector area of interest earlier than the left-running wave. Also, it can be deduced that the right-running wave is faster in this particular case than the left-running wave. Finally, at x2, both waves have collided and the amplitude reaches the peak value at around t=40μs.

The visualization images, presented in Fig. 5.14, are used to better understand the pressure traces taken during the interaction process captured in Fig. 5.13. In the first phase, two detonation waves approach the injector bank from both sides and collide near the injector #5. At this point in time, since there is no more unburned reactants left in the channel, the detonation waves decay and turn into blast waves. As the waves move further away from each other, their wave speeds continue to decrease. Near the very location of the two waves colliding, the affected injectors are subjected to a higher peak pressure as the ambient gases are compressed twice before any expansion. The injectors further away are subjected not only to a weaker-amplitude second-arriving wave but it also arrives after the compression effect of the first wave from the opposite side decays. However, the combined effect of the weaker waves with a delayed arrival leads to a slower refresh of the affected injectors than those injectors near the wave collision point. In other words, the synchronized arrival of the two counter-propagating waves causes a higher peak pressure amplitude locally but it also leads to a faster pressure relaxation resulting in a quicker injection refresh.

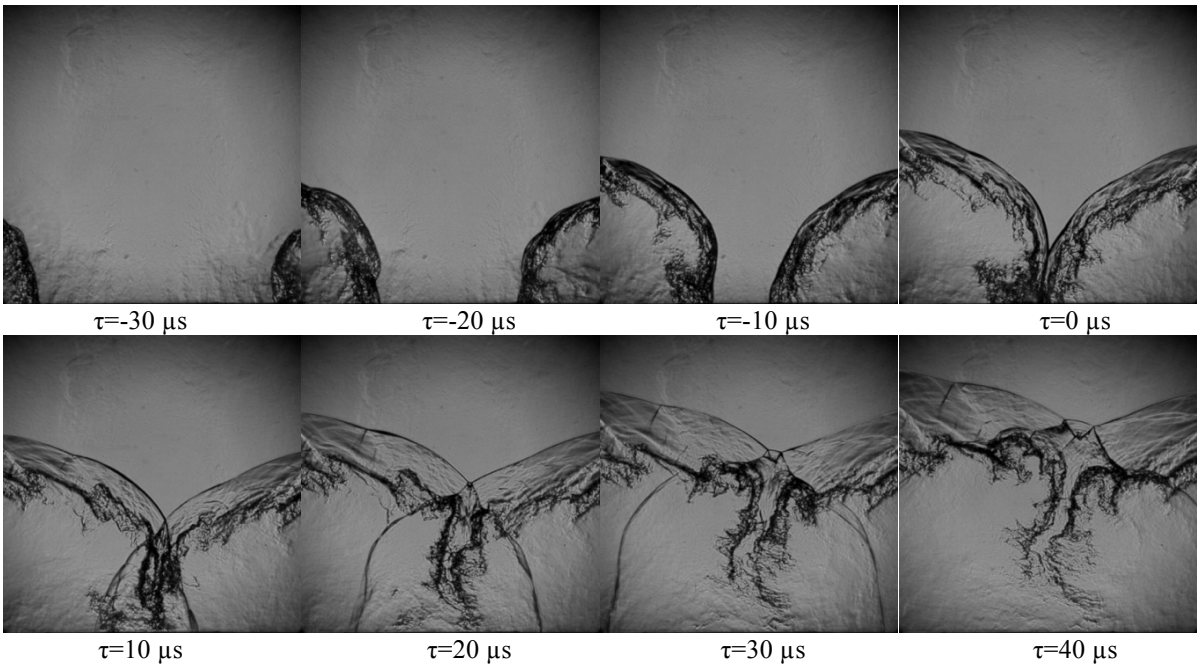

Fig. 5.14. Sequence of images showing two counter-propagating waves colliding over the injectors.

Figure 5.15 shows the injector refresh behavior following the wave collision. Fig. 5.15 (a) shows the first set of refresh jets that start at about 350 μs after the time of wave collision. This time delay is significantly longer than the single wave cases, in which a similar mass flow rate was injected into the combustor (Case 1-N). Also, each injector response is different since they were exposed to a different pressure field following various patterns of the two wave passages, depending on the location of the injector. For the single-wave cases, the refresh patterns from a bank of adjacent injectors are quite similar. The refresh jets line up monotonically following the wave passage direction. For the cases involving counter-propagating waves, However, the refresh jet closest to the collision location recovered more quickly than the refresh jets from other injectors away from the collision point.

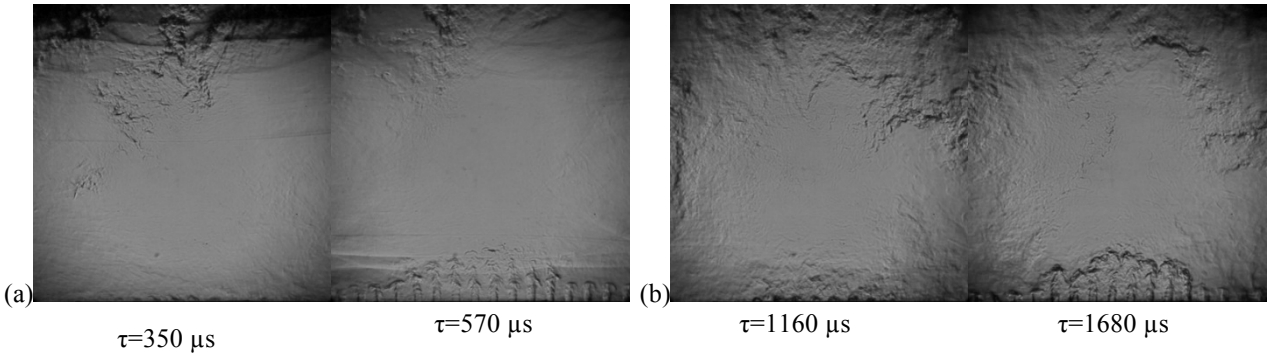

Fig. 5.15. Injector refresh after wave collision. (a) The first refresh starts at 350 μs after the collision, and (b) the second refresh starts at 1160 μs after the collision.

The response of refresh jets entering a linear channel from the base is investigated, while the channel flow is subjected to various detonation waves that propagate along the channel. The channel geometry represents an unwrapped RDE combustor, and the refresh jets are supposed to simulate those reactant jets entering the combustor during a typical operation. In this work, the results with non-reacting jets are presented. Detonation waves are established inside the channel using two pre-detonation tubes, which are mounted at each end of the channel. Since the injection jets are non-reacting, detonation waves quench over the jet flow-field setting up decaying blast waves over the injectors. As a result, the wave strength decreases over those injectors that are further away from the origin of the blast waves. Finally, the jet refresh behaviors including the characteristic delay time and the initial velocity at the onset of refresh are experimentally measured as a function of wave strength, wave interaction, and refresh jet flow rate.

For the case of refresh jets interacting with a single wave, the results show that the refresh delay time depends on both the jet flow rate and the wave strength. Under certain conditions, however, the refresh delay time is more uniform across the injectors, relatively less affected by the injector location or the wave strength. For most other conditions, the refresh delay time decreases with the jet flow rate and increases with the wave strength.

For the case of counter-propagating waves colliding over the test section, each refresh jet is subjected to a different type of pressure waves depending on its relative location with respect to the point of wave collision. At the point of colliding waves, the refresh jet is subjected to the similar type of pressure wave as in the single wave case. Other adjacent jets, however, are subjected to a double-peaked pressure pulse that affected their recovery characteristics. The refresh jet at the point of collision recovers the first, followed by those jets with smaller time delay between the pressure peaks. The results provide enhanced understanding of the physical processes inside an RDE combustor during a slapping-mode operation.

REFERENCES

[1] Wolanski, P., Kindracki, J., Fujiwara, T., Oka, Y, Shimauchi, K., "An Experimental Study of Rotating Detonation Engine," *20th ICDERS*, Montreal, Canada (2005)

[2] Bykovskii, F., Zhdan, S., Vedernikov, E., "Continuous Spin Detonations," *Journal of Propulsion and Power*, Vol.22, p.1204-1216, (2006)

[3] Hishida, M., Fujiwara, T. and Wolanski, P., "Fundamentals of rotating detonation," *Shock Waves*, Vol.19, p.1-10, (2009)

[4] Schwer, D., Kailasanath, K., "Numerical investigation of the physics of rotating-detonation-engines," *Proc. of the Combustion Institute*, Vol.33, p.2195-2202, (2011)

[5] Schauer, F., "Pulse Detonation Physiochemical and Exhaust Relaxation Processes," *AFOSR-ARO Basic Combustion Research Review Meeting*," Arlington, VA (2012)

[6] Fievisohn, R., and Yu, K.H., "Steady-State Analysis of Rotating Detonation Engine Flowfields with the Method of Characteristics," *Journal of Propulsion and Power*, Vol.33 (1), pp. 89-99, (2017)

[7] Wintenberger, E., Shepherd, J. E., "Thermodynamic cycle analysis for propagating detonations," *Journal of Propulsion and Power*, Vol.22(3), 694-697, (2006)

[8] Fievisohn, R., "," Ph.D. Thesis, Aerospace Engineering, University of Maryland, College Park, MD, (2020); DOI: https://doi.org/10.13016/uvxz-40cv, URI: http://hdl.handle.net/1903/19071

[9] Burr, J., "Fundamental Study of Detonation Structure in Rotating Detonation Engine," Ph.D. Thesis, Aerospace Engineering, University of Maryland, College Park, MD, (2020); DOI: https://doi.org/10.13016/uvxz-40cv, URI: http://hdl.handle.net/1903/26264

[10] Shank J., "Development and Testing of Rotating Detonation Engine Run on Hydrogen and Air", MS Thesis, Air Force Institute of Technology, Wright-Patterson AFB, OH, (2012)

[11] Schwer D., Kailasanath K., "Feedback into Mixture Plenums in RDE", 51st AIAA Aerospace Sciences Meeting, AIAA-2012-0617, (2012)

[12] Redhal, S., Burr, J., and Yu, K.H., "Injector Flowfield-Detonation Wave Interaction in Unwrapped RDE Channel" *AIAA Propulsion and Energy Forum*, AIAA-2019-4216, August (2019); DOI: https://doi.org/10.2514/6.2019-4216

[13] Chang, M., Redhal, S., Burr, J. R., & Yu, K.H., "Detonation Wave-Refresh Jet Interaction in Unwrapped RDE Combustor", AIAA SciTech 2021 Forum, AIAA-2021-1379, January (2021); DOI: https://doi.org/10.2514/6.2021-1379

6.0 PUBLICATIONS, AWARDS, AND PERSONNEL

6.1.Publications

[1] Burr, J.R., and Yu, K.H., "Experimental Characterization of RDE Combustor Flowfield Using Linear Channel," *Proc. of Combustion Institute*, Vol. 37 (3), pp. 3471-3478 (2019). DOI: https://doi.org/10.1016/j.proci.2018.09.001

[2] Prakash, S., Fiévet, R., Raman, V., Burr, J., and Yu, K.H. "Analysis of the Detonation Wave Structure in a Linearized Rotating Detonation Engine," *Journal of AIAA*, published online: 8 Oct. (2019) DOI: https://doi.org/10.2514/1.J058156

[3] Fievisohn, R., and Yu, K.H., "Steady-State Analysis of Rotating Detonation Engine Flowfields with the Method of Characteristics," *Journal of Propulsion and Power*, Vol. 33 (1), pp. 89-99, (2017). DOI: https://doi.org/10.2514/1.B36103

[4] Lu, F.K., Miller, R., Nalim, M.R., and Yu, K.H., "Introduction: Special Section on Pressure Gain Combustion," *Journal of Propulsion and Power*, Vol. 33 (1), p.16, (2017). DOI: https://doi.org/10.2514/1.B36585

[5] Chang, M., Redhal, S., Burr, J. R., & Yu, K.H., "Detonation Wave-Refresh Jet Interaction in Unwrapped RDE Combustor", *AIAA SciTech 2021 Forum*, AIAA-2021-1379, January (2021); DOI: https://doi.org/10.2514/6.2021-1379

[6] Redhal, S., Burr, J., and Yu, K.H. "Fuel Injection, Mixing, and Detonative Combustion in Model Detonation Engine," *24th International Society of Air Breathing Engines Conference*, ISABE-2019-24254, September (2019)

[7] Redhal, S., Burr, J., and Yu, K.H., "Injector Flowfield-Detonation Wave Interaction in Unwrapped RDE Channel" *AIAA Propulsion and Energy Forum*, AIAA-2019-4216, August (2019); DOI: https://doi.org/10.2514/6.2019-4216

[8] Burr, J. and Yu, K.H., "Characterization of CH4-O2 Detonation in Unwrapped RDE Channel Combustor" *AIAA Propulsion and Energy Forum*, AIAA-2019-4215, August (2019); DOI: https://doi.org/10.2514/6.2019-4215

[9] Burr, J. and Yu, K.H., "Characterization of Detonation Wave Heat Release and RDE Mode Selection" 27th International Colloquium on the Dynamics of Explosions and Reactive Systems, Beijing, China, Paper No. 351, July (2019); http://www.icders.org/ICDERS2019/abstracts/ICDERS2019-351.pdf

[10] Redhal, S., Burr, J., and Yu, K.H., "Fuel Injection Dynamics and Detonation Wave Interaction in Rectangular Channel," *AIAA SciTech 2019 Forum*, AIAA-2019-2251, January (2019); DOI: https://doi.org/10.2514/6.2019-2251

[11] Burr, J., and Yu, K.H. "Mixing in Linear Detonation Channel with Discrete Injectors and Side Relief," *57th AIAA Aerospace Sciences Meeting, AIAA SciTech 2019 Forum*, AIAA-2019-1014, January (2019); DOI: https://doi.org/10.2514/6.2019-1014

[12] Burr, J., and Yu, K., "Investigation of Rotating Detonation Engine Cycle Using Linear Model Combustor," *2018 International Workshop on Detonation for Propulsion*, Xi'an, China, September (2018)

[13] Redhal, S., Burr, J., and Yu, K.H., "Fuel Injection, Mixing and Combustion in Model Rotating Detonation Engine," *22nd AIAA International Space Planes and Hypersonic Systems and Technologies Conference*; *AIAA SPACE Forum*, AIAA-2018-5200, September (2018); DOI: https://doi.org/10.2514/6.2018-5200

[14] Burr, J., and Yu, K.H., "Impulsively Started Ethylene-Oxygen Injection in Linear Channel Following Detonation Wave Passage," *54th AIAA/SAE/ASEE Joint Propulsion Conference*; *AIAA Propulsion & Energy Forum*, AIAA-2018-4570, July (2018); DOI: https://doi.org/10.2514/6.2018-4570

[15] Prakash, S., Fievet, R., Raman, V., Burr, J., and Yu, K.H. "Numerical Study of the Detonation Wave Structure in a Linear Model Detonation Engine," *56th AIAA Aerospace Sciences Meeting, AIAA SciTech Forum*, AIAA-2018-4966, January (2018); DOI: https://doi.org/10.2514/6.2018-4966

[16] Burr, J., and Yu, K.H. "Detonation Wave Propagation in Discretely Spaced Hydrocarbon Cross-flow," *56th AIAA Aerospace Sciences Meeting, AIAA SciTech Forum*, AIAA-2018-1420, January (2018); DOI: https://doi.org/10.2514/6.2018-1420

[17] Burr, J.R., and Yu, K.H., "Detonation Propagation in a Linear Channel with Discrete Injectors and Side Relief," *26th International Colloquium on the Dynamics of Explosions and Reactive Systems*, ICDERS 2017-1107, July-August (2017); http://www.icders.org/ICDERS2017/abstracts/ICDERS2017-1107.pdf

[18] Burr, J., and Yu, K.H., "Detonation Wave Propagation in Cross-Flow of Discretely Spaced Reactant Jets," *53rd AIAA/SAE/ASEE Joint Propulsion Conference*; *AIAA Propulsion & Energy Forum*, AIAA-2017-4908, July (2017); DOI: https://doi.org/10.2514/6.2017-4908

[19] Schwer, D., Kailasanath, K., Burr, J., and Yu, K., "Simulations of the Linear Model Detonation Engine," *10th U.S. National Combustion Meeting*, Combustion Institute, April (2017)

[20] Burr, J., Yu, K.H., Schwer, D., and Kailasanath, K. "Experiments in the Linear Model Detonation Engine," *10th U.S. National Combustion Meeting*, Combustion Institute, April (2017)

6.2. Awards

Shikha C. Redhal,	received *Outstanding Research Assistant Award*, University of Maryland Graduate School, awarded on December 22, (2020)
Shikha C. Redhal,	received *Zonta International Amelia Earhart Award*, Zonta International Foundation, awarded on October 5, (2019)
Jason R. Burr,	received *Best Doctoral Research Award* in Aerospace Engineering, UMD A. James Clark Engineering School, awarded on April 30, (2019)
Kenneth H. Yu,	inducted to *ASME Fellow*, American Society of Mechanical Engineers, (2017)
Robert T. Fievisohn	received *Best Doctoral Research Award* in Aerospace Engineering, UMD A. James Clark Engineering School, awarded on April 20, (2016)
Robert T. Fievisohn	received *AIAA Martin Summerfield Propellants & Combustion Graduate Award*, American Institute of Aeronautics and Astronautics, (2015)

6.3. Personnel

Kenneth H. Yu	Associate Professor, Department of Aerospace Engineering, University of Maryland
Jason Burr	Graduate Research Assistant, Aerospace Engineering Ph.D., conferred 2020
Robert Fievisohn	Graduate Research Assistant, Aerospace Engineering Ph.D., conferred 2016
Shikha Redhal	Graduate Research Assistant, Department of Aerospace Engineering Degree Goal: Ph.D.
Minwook Chang	Graduate Research Assistant, Department of Aerospace Engineering Degree Goal: Ph.D.

6.4. Degrees Awarded

Jason Burr	Ph.D. in Aerospace Engineering, University of Maryland, May 2020 Thesis entitled "Fundamental Study of Detonation Structure in Rotating Detonation Engine," (Placement: Air Force Research Lab; AFRL/RQ Edwards AFB)
Robert Fievisohn	Ph.D. in Aerospace Engineering, University of Maryland, December 2016 Thesis entitled "Development and Application of Theoretical Models for Rotating Detonation Engine Flowfields," (Placement: Air Force Research Lab; AFRL/RQ Wright-Patterson AFB)
Shikha Redhal	M.S. in Aerospace Engineering, University of Maryland, May 2019 Scholarly paper entitled "Fuel Injection Dynamics and Detonation Wave Interaction in Rectangular Channel," (continued to the Ph.D. program)